EUROPEAN ORGANIZATION FOR NUCLEAR RESEARCH (CERN)

CERN-EP-2024-043
2024/08/20

CMS-HIG-21-005

Search for Higgs boson pair production in the $b\bar{b}W^+W^-$ decay mode in proton-proton collisions at $\sqrt{s} = 13\,\text{TeV}$

The CMS Collaboration*

arXiv:2403.09430v2 [hep-ex] 18 Aug 2024

Abstract

A search for Higgs boson pair (HH) production with one Higgs boson decaying to two bottom quarks and the other to two W bosons are presented. The search is done using proton-proton collisions data at a centre-of-mass energy of 13 TeV, corresponding to an integrated luminosity of 138 fb^{-1} recorded by the CMS detector at the LHC from 2016 to 2018. The final states considered include at least one leptonically decaying W boson. No evidence for the presence of a signal is observed and corresponding upper limits on the HH production cross section are derived. The limit on the inclusive cross section of the nonresonant HH production, assuming that the distributions of kinematic observables are as expected in the standard model (SM), is observed (expected) to be 14 (18) times the value predicted by the SM, at 95% confidence level. The limits on the cross section are also presented as functions of various Higgs boson coupling modifiers, and anomalous Higgs boson coupling scenarios. In addition, limits are set on the resonant HH production via spin-0 and spin-2 resonances within the mass range 250–900 GeV.

Published in the Journal of High Energy Physics as doi:10.1007/JHEP07(2024)293.

© 2024 CERN for the benefit of the CMS Collaboration. CC-BY-4.0 license

*See Appendix A for the list of collaboration members

1 Introduction

In 2012, the ATLAS and CMS Collaborations at the CERN LHC discovered a new particle with a mass of approximately 125 GeV [1–3]. According to all current measurements, it is compatible with the standard model (SM) Higgs boson (H) [4–7]. An important pending test of the electroweak symmetry breaking mechanism is the observation of Higgs boson pair (HH) production. At the LHC, pairs of SM Higgs bosons are primarily produced via gluon-gluon fusion (ggF), with a cross section of $31.1^{+2.1}_{-7.2}$ fb at 13 TeV centre-of-mass energy [8–12]. At leading order (LO), two destructively interfering Feynman diagrams contribute, the "triangle diagram" and the "box diagram", shown in Fig. 1. The triangle-diagram gives direct access to the Higgs boson trilinear coupling λ_{HHH}, which affects the shape of the Higgs field potential. A secondary production mechanism for HH events is the vector boson fusion (VBF) shown in Fig. 2. While the cross section of the VBF production is smaller, only 1.726 ± 0.036 fb in the SM at 13 TeV [13], it gives experimental access to the quartic HHVV coupling (where V is a W or Z boson). The HH production is also sensitive to other Higgs boson couplings, such as the HVV coupling. The Higgs boson couplings are described by their coupling modifiers, the ratio between the measured coupling strength and the prediction in the SM, noted with κ [14]. For example κ_λ is the coupling modifier corresponding to the Higgs boson trilinear coupling and κ_t is the coupling modifier between a Higgs boson and a top quark. Beyond the SM, there may be additional diagrams contributing to HH production that include couplings not predicted in the SM. The anomalous couplings studied in the present paper are denoted c_i and shown in Fig. 3. Here c_2 corresponds to the coupling between two top quarks and two Higgs bosons, c_g corresponds to the coupling between a Higgs boson and two gluons, and $c_{2\mathrm{g}}$ corresponds to the coupling between two Higgs bosons and two gluons.

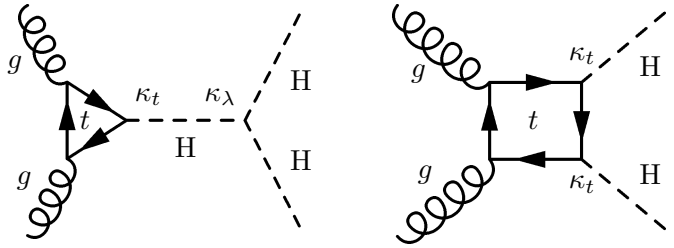

Figure 1: Leading-order Feynman diagrams of nonresonant Higgs boson pair production via gluon fusion in the standard model.

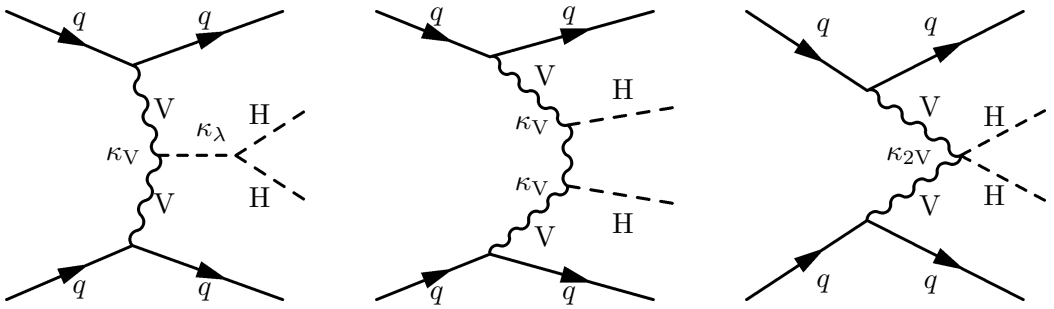

Figure 2: Leading-order Feynman diagrams of Higgs boson pair nonresonant production via vector boson fusion in the standard model.

The HH production could also be enhanced by resonant contributions through the production of a new heavy resonance (X) decaying to a pair of Higgs bosons. Examples of such new resonances include a radion [15], a heavy CP-even scalar in two-Higgs-doublet models [16] and a spin-2 graviton in the bulk Randall–Sundrum model [17, 18].

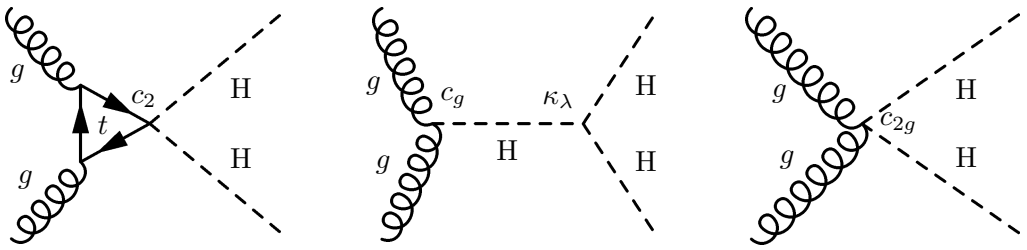

Figure 3: Leading-order Feynman diagrams of nonresonant Higgs boson pair production via gluon fusion with anomalous Higgs boson couplings.

This paper describes a search for nonresonant and resonant HH production in the decay channel to a pair of b quarks and a pair of W bosons. The search is carried out by analysing proton-proton (pp) collision data recorded by the CMS detector [19] from 2016 to 2018 at 13 TeV centre-of-mass energy with single- and double-lepton triggers. The data sample corresponds to an integrated luminosity of 138 fb^{-1} [20–22].

The $\text{HH} \to \text{b}\bar{\text{b}}\text{W}^+\text{W}^-$ decay has the second-largest branching fraction, following the $\text{HH} \to \text{b}\bar{\text{b}}\text{b}\bar{\text{b}}$ decay. We consider events with at least one W boson decaying to an electron or a muon. Higgs boson decays to a pair of tau leptons with subsequent decay of both tau leptons to electrons or muons, as well as Higgs boson decays to a pair of Z bosons resulting in a final state with two electrons or muons, are also considered as signal. From here on in this paper, the term leptons is used for electrons and muons unless explicitly stated otherwise. The main backgrounds contributing to this final state are the top quark pair production ($\text{t}\bar{\text{t}}$+jets), followed by the Drell–Yan (DY) or W+jets processes depending on whether the second W boson decays leptonically or hadronically, respectively. In the latter case, events with misidentified leptons represent a sizeable contribution. Other SM processes contribute to a lesser extent, for example single top quark and multiboson (VV and VVV) productions.

The combination of HH nonresonant searches by the CMS Collaboration [5] sets an upper limit on the inclusive HH production cross section observed (expected) at 3.4 (2.5) times the theoretical cross section predicted by the SM, at 95% confidence level (CL). The coupling modifier for the trilinear Higgs boson self-coupling, κ_λ, is excluded outside the range -1.25 and 6.85, at 95% CL, using the modified frequentist CL_s method [23, 24]. The coupling modifier for the quartic interaction between two Higgs bosons and two W or Z bosons, $\kappa_{2\text{V}}$, is excluded outside the range 0.67 and 1.38, at 95% CL, which corresponds to an exclusion of the $\kappa_{2\text{V}} = 0$ hypothesis by 6.6 standard deviations, when all other couplings are assumed to be SM-like. These results include several HH decays but not $\text{b}\bar{\text{b}}\text{W}^+\text{W}^-$, namely $\gamma\gamma\text{b}\bar{\text{b}}$, $\text{b}\bar{\text{b}}\text{b}\bar{\text{b}}$, $\tau\tau\text{b}\bar{\text{b}}$, $\text{ZZb}\bar{\text{b}}$ and final states with leptons. The ATLAS Collaboration published a combination of HH results, including $\gamma\gamma\text{b}\bar{\text{b}}$, $\text{b}\bar{\text{b}}\text{b}\bar{\text{b}}$ and $\tau\tau\text{b}\bar{\text{b}}$ decays, constraining the observed (expected) HH production to 2.4 (2.9) times the SM value, at 95% CL [25]. The ATLAS Collaboration has also published a result on the $\text{HH} \to \text{b}\bar{\text{b}}\text{W}^+\text{W}^-$ channel in final states with two leptons [26]. This search constrained the observed (expected) inclusive HH production cross section to be lower than 9.7 (16.2) times the SM cross section, at 95% CL. The most recent result on $\text{HH} \to \text{b}\bar{\text{b}}\text{W}^+\text{W}^-$ by the CMS Collaboration [27] used only the data collected in 2016, corresponding to an integrated luminosity of 35.9 fb^{-1} and reported an observed (expected) exclusion limit at 79 (89) times the value predicted by the SM. The analysis presented in this paper improves this result by up to a factor 5. Besides the additional data from 2017–2018 used in this paper, the previous analysis considered only the fully leptonic $\text{H} \to \text{W}^+\text{W}^-$ decays while here the semileptonic decay is considered as well. The case of a highly Lorentz-boosted $\text{H} \to \text{b}\bar{\text{b}}$ decay is also considered for the first time in this decay channel. The sensitivity is further improved by the use of a better

algorithm [28] for identifying jets originating from b quarks and a different machine learning strategy for signal extraction.

This paper is structured as follows: the apparatus and the simulated samples are described in Section 2 and Section 3. Section 4 summarises the physics object reconstruction and identification. Event selection and analysis strategy are discussed in Section 5 and Section 6. We then discuss the background estimation and the systematic uncertainties in Section 7 and Section 8. Finally, Section 9 presents the results, and Section 10 the summary. A HEPData record is provided for the results [29].

2 The CMS detector

The central feature of the CMS apparatus is a superconducting solenoid of 6 m internal diameter, providing a magnetic field of 3.8 T. Within the solenoid volume, there is a silicon pixel and strip tracker, a lead tungstate crystal electromagnetic calorimeter (ECAL), and a brass and scintillator hadron calorimeter (HCAL), each composed of a barrel and two endcap sections. Forward calorimeters extend the pseudorapidity (η) coverage provided by the barrel and endcap detectors. Muons are measured in gas-ionisation detectors embedded in the steel flux-return yoke outside the solenoid.

A more detailed description of the CMS detector, together with a definition of the coordinate system used and the relevant kinematic variables, can be found in Ref. [19].

Events of interest are selected using a two-tiered trigger system. The first level, composed of custom hardware processors, uses information from the calorimeters and muon detectors to select events at a rate of around 100 kHz within a time interval of less than 4 μs [30]. The second level, known as the high-level trigger, consists of a farm of processors running a version of the full event reconstruction software optimised for fast processing, and reduces the event rate to around 1 kHz before data storage [31].

3 Simulated samples

The parton showering, hadronisation processes, and decays of τ leptons, including polarisation effects, are modelled using the generator PYTHIA 8.230 [32] with the tune CUETP8M1 [33] for the 2016 data-taking period, and with the tune CP5 [34] for the 2017–2018 data-taking periods. The simulated samples produced by PYTHIA with the CUETP8M1 tune use the NNPDF3.0 parton distribution functions (PDFs), whereas the samples produced with the CP5 tune use the NNPDF3.1 set [35–37]. Finally, the samples produced by MADGRAPH5_aMC@NLO 2.2.2 [38–40] and POWHEG v2 [41–43], use the NNPDF3.1 set.

The response of the CMS detector is modelled using the GEANT4 toolkit [44]. Additional pp interactions in the same or nearby bunch crossings, referred to as pileup, are simulated using PYTHIA and overlaid on the simulated events using event weights so that the distribution of the number of collisions matches the data.

3.1 HH signal modelling

The HH signal samples for nonresonant ggF production are generated using next-to-leading-order (NLO) matrix elements implemented in the POWHEG program. These samples are produced in four benchmark hypotheses with varying values of the κ_λ modifier ($\kappa_\lambda = 0$, $\kappa_\lambda = 2.45$, $\kappa_\lambda = 5.0$, and $\kappa_\lambda = 1$ (SM)), while the others are kept to their SM expected values. The

dependence of the ggF HH cross section on κ_λ and κ_t can be obtained from three terms corresponding to the diagrams involving κ_λ, κ_t, and the interference [45]. Therefore we can model any kinematic distribution of the ggF production over a large range of κ_λ and κ_t values using a weighted sum of three of the four generated samples. Each weighted sum of samples is then normalised to the corresponding next-to-NLO (NNLO) cross section [12].

In order to study further modified values for the SM couplings as well as couplings not present in the SM we use an event-based reweighting method. The reweighting is based on a parameterisation of the differential cross section on the generator-level invariant mass of the HH system and the angular distance between the two Higgs bosons in the azimuthal plane, which are sufficient to characterize the hard scattering that only has two degrees of freedom. It allows to access any combination of coupling modifiers (κ_λ, κ_t, c_2, c_g, c_{2g}), even for values that were not used in the sample generation.

The modelling of the VBF process follows the same principle. In this case, the samples are generated at LO with MADGRAPH5_aMC@NLO. Seven benchmark samples are generated with varying values of coupling modifiers κ_λ, κ_V and κ_{2V}. The cross section depends on six terms that are combinations of these three coupling modifiers. Accordingly, six of the seven generated samples are used in the weighted combination.

The simulated samples for resonant HH production are produced using LO matrix elements implemented in the MADGRAPH5_aMC@NLO. The resonances are assumed to be in the mass range 250–900 GeV, have narrow width compared to the experimental resolution, and have spin 0 or 2.

3.2 Background simulation

Simulated samples for the $t\bar{t}$+jets, single top quark production and WW processes are generated by POWHEG at NLO. The simulated transverse momentum (p_T) spectrum of the top quarks is harder than the one observed in data. Therefore, we compute a correction which is then applied to the $t\bar{t}$+jets Monte Carlo samples. The top quark p_T is weighted by the ratio of the NNLO theoretical cross section over the cross section obtained from simulation [46]. Single Higgs boson and ZZ backgrounds are simulated either by POWHEG or MADGRAPH5_aMC@NLO at NLO depending on the production mechanism and the subsequent decay. The DY, W+jets, $t\bar{t}W/Z$ and WZ and all VVV processes are generated at NLO with MADGRAPH5_aMC@NLO. The DY and W+jets backgrounds are modelled using "inclusive" samples, covering the whole phase space, and complementary DY and W+jets samples binned in the multiplicity of jets at generator level. The "stitching" of the different DY and W+jets samples is documented in Ref. [47]. Additional DY samples produced using LO matrix elements implemented in MADGRAPH5_aMC@NLO are used when training the machine learning algorithms implemented in this analysis in order to reduce the statistical uncertainty. The DY, W+jets, and $t\bar{t}$+jets samples are normalised to cross sections computed at NNLO accuracy [48–50]. The Wγ+jets, $t\gamma$+jets and other rare processes are simulated at LO with MADGRAPH5_aMC@NLO.

4 Physics object reconstruction and identification

4.1 Particle-flow algorithm

The particle-flow (PF) algorithm [51] aims to reconstruct and identify each particle (PF candidate) in an event, with an optimised combination of information from the various elements of the CMS detector. These reconstructed particles are the so-called PF candidates and are classified as electrons, muons, photons, and charged or neutral hadrons. The energy of electrons is

determined from a combination of the track momentum at the primary vertex, the corresponding ECAL cluster energy, and the energy sum of all bremsstrahlung photons attached to the track. The momentum of muons is obtained from the curvature of the corresponding track. The energy of charged hadrons is determined from a combination of their momentum measured in the tracker and the matching ECAL and HCAL energy deposits, corrected for the response function of the calorimeters to hadronic showers. Finally, the energy of neutral hadrons is obtained from the corresponding corrected ECAL and HCAL energies. The PF candidates are the starting point for further object identification and are used to build more complex objects like jets, and missing transverse momentum. The primary vertex is taken to be the vertex corresponding to the hardest scattering in the event, evaluated using tracking information alone, as described in Section 9.4.1 of Ref. [52].

4.2 Small-radius jets

Small-radius jets are reconstructed from PF candidates, using the anti-k_T clustering algorithm [53, 54] with a distance parameter of $R = 0.4$. Charged particles not originating from the primary vertex are excluded from the jet clustering. The energy of reconstructed jets is calibrated as a function of jet p_T and η [55, 56]. Corrections based on the area and energy density of the jet are applied in order to compensate for effects from pileup. The jets selected in this analysis are required to satisfy the conditions $p_T > 25\,\text{GeV}$ and $|\eta| < 2.4$, as well as selection criteria to remove jets adversely affected by instrumentation or reconstruction failure. In order to reduce the number of jets originating from pileup among the jets with $p_T < 50\,\text{GeV}$, a set of criteria is applied to the compatibility of the tracks associated with the jet with the primary vertex, the topology of the jet shape, and the track multiplicity [57]. All selected jets are required not to overlap with electrons or muons passing the medium selection defined in Section 4.4.3 within $\Delta R = \sqrt{(\Delta\eta)^2+(\Delta\phi)^2} < 0.4$. We refer to these jets as "small-radius jets".

A deep neural network (DNN) based algorithm, DEEPJET [28], is applied to identify small-radius jets originating from the hadronisation of b quarks ("b tagging"). The medium working point that yields an efficiency of 75% for identifying jets from b quarks (b jets), with a 1% (10%) misidentification rate for jets from light-flavour (charm) quarks and gluons, is used throughout this analysis [58]. This DNN-based algorithm exploits observables related to the long lifetime of b hadrons and the high charged particle multiplicity and mass of b jets compared to light quark and gluon jets. Corrections are derived from data enriched in b jets, in order to account for the difference in data and simulation efficiencies, as a function of the jet p_T, $|\eta|$ and the algorithm output score. They are applied to simulated events to improve the agreement with the data in the whole range of algorithm output scores [58]. The estimation of the b jet energy can be biased by the presence of neutrinos in semileptonic decays within the jet and by the detector response. To correct for this, a DNN regression algorithm is trained on jet composition and shape information and applied to b-tagged jets, improving the energy resolution by 12–15% [59].

To improve the sensitivity to the VBF production with its forward jets, an additional category of jets (referred to as VBF jets) is considered with similar selections except for $p_T > 30\,\text{GeV}$ and $|\eta| \leq 4.7$. During the 2017 data-taking period, jets and unclustered PF candidates with $2.650 < |\eta| < 3.139$ and $p_T < 60\,\text{GeV}$ are rejected to reduce the effect of the noise in the ECAL endcap at high $|\eta|$.

4.3 Large-radius jets

Decays of high-p_T Higgs bosons into a pair of b quarks result in final states with large Lorentz boost and as a result, the b jets can be overlapping, forming one jet with large R ("large-radius

jet") and substructure (i.e. the two overlapping jets are "subjets" of the large-radius jet). These jets are reconstructed using the anti-k_T algorithm with a distance parameter $R = 0.8$. Contributions from pileup are reduced by weighting the PF particles used as input to the reconstruction of large-radius jets with the "pileup-per-particle identification" algorithm [60].

The large-radius jets are required to not be within $\Delta R < 0.8$ from leptons passing the medium selection defined in Section 4.4.3, and to have $p_T > 200\,\text{GeV}$ and $|\eta| < 2.4$. The two subjets are required to have $p_T > 20\,\text{GeV}$. At least one of the subjets is required to have $p_T > 30\,\text{GeV}$ and pass the medium b tagging working point of the DEEPCSV algorithm [61], with a b jet efficiency of 68% and misidentification rate of 1% for light-flavour and gluon jets. Similarly to the small-radius jets, a correction derived from data is applied to simulated events to account for the differences in selection efficiencies associated with the medium working point. The soft-drop mass (m_{SD}) of the large-radius jet is reconstructed using the modified mass drop tagger (also known as the "soft-drop" (SD)) algorithm [62, 63], with an angular exponent $\beta = 0$, soft-cutoff threshold $z_{cut} < 0.1$, and characteristic radius $R_0 = 0.8$. This quantity is designed to remove soft and wide-angle radiation from the large-radius jet and is required to be within the range $30 < m_{SD} < 210\,\text{GeV}$. The N–subjettiness [64] τ_N denotes a quantity that measures the alignment of the jet energy along the axes of candidate subjets and is interpreted as the compatibility of a jet to have N subjets. The ratio $\tau_2/\tau_1 < 0.75$ quantifies the compatibility of the large-radius jet with the two-prong structure expected from the decay of a W, Z or Higgs boson into two quarks. This ratio is used in this analysis in the discrimination of $H \to b\bar{b}$ decays of a Lorentz-boosted Higgs boson from quark and gluon jets.

4.4 Electrons and Muons

The electron and muon selection is performed in two stages. The first stage is the identification and isolation of genuine electron and muon candidates. The second stage is the selection of leptons specifically for the different aspects of this analysis, namely signal selection and background estimation or rejection.

4.4.1 Electron and muon identification

The first step of the electron identification is performed by a multivariate analysis (MVA) algorithm [65, 66] based on a boosted decision tree [67] which is trained to discriminate electrons against jets. In this analysis, we use the selection threshold with 90% efficiency for prompt electrons originating from the primary vertex. Electron candidates arising from photon conversions are suppressed by requiring that the track is missing no more than one hit in the innermost layers of the silicon tracker and is not matched to a reconstructed conversion vertex.

The first step of the muon identification consists of linking track segments reconstructed in the silicon tracking detector with those in the muon system [68]. Quality requirements are applied on the multiplicity of hits, the number of matched segments and the quality of the global muon track fit, quantified by its normalized χ^2. The muon candidates used in the analysis are required to pass the "loose" PF muon identification criteria [69], which guarantee more than 99% efficiency over the entire η range. The probability of pions or kaons to be misidentified as "loose" muons is about 0.2% and 0.5% respectively.

4.4.2 Electron and muon isolation

Electrons and muons in signal events are expected to be isolated. Lepton isolation is defined as scalar p_T sum of all charged particles, neutral hadrons, and photons reconstructed within a narrow cone centred on the lepton direction. The size R of the cone is inversely proportional to

the p_T of the lepton, causing increased efficiency for passing the isolation criteria for leptons reconstructed in events with overlapping jets due to high Lorentz boost or high hadronic activity. R varies from 0.05 for leptons with $p_T > 200\,\text{GeV}$ to 0.20 for leptons with $p_T < 50\,\text{GeV}$. Only charged particles originating from the lepton production vertex are considered in the isolation sum. Residual contributions of pileup to the neutral component of the isolation of the lepton are taken into account using effective-area corrections:

$$I^{\text{lep}} = \sum_{\text{charged}} p_T + \max\left(0, \sum_{\text{neutral}} p_T - \rho\,\mathcal{A}\,\left(\frac{R}{0.3}\right)^2\right), \tag{1}$$

where ρ represents the energy density of neutral particles reconstructed within the geometric acceptance of the tracking detectors, computed as described in Refs. [70, 71]. The leptons considered are required to have $I^{\text{lep}}/p_T^{\text{lep}} < 0.4$. The effective area $\mathcal{A}$ is obtained from simulation by studying the correlation between I^{lep} and ρ. It is determined separately for electrons and muons in bins of η.

4.4.3 Signal lepton selection

The analysis utilises three different levels of lepton selection criteria with increasing tightness for electrons and muons, to which we refer to as the loose, medium and tight lepton selections.

The loose selection is used to remove lepton pair resonances. Requirements are the following: $p_T > 5\,\text{GeV}$ (7 GeV) and $|\eta| < 2.5$ (2.4) for electrons (muons); isolation $I^{\text{lep}}/p_T^{\text{lep}} < 0.4$; impact parameters of the lepton track with respect to the primary vertex, transverse $|d_{xy}| < 0.05\,\text{cm}$ and longitudinal $|d_z| < 0.1\,\text{cm}$; significance of the impact parameter $d/\sigma_d < 8$ in three dimensions (3D).

The medium lepton selection is used for removing the overlap between different types of objects, for certain variables in the event preselection and the misidentified-lepton background estimate based on control samples in data. The p_T of medium leptons is set to the p_T^{cone}, as this has been found to describe better the p_T of misidentified leptons. The p_T^{cone} is defined as 0.9 times the p_T of the nearest jet if they are within $\Delta R < 0.4$, otherwise as $0.9(p_T^{\text{lep}} + I^{\text{lep}})$, where I^{lep} is the lepton isolation given by Eq. (1). The p_T^{cone} in general exceeds the p_T of the lepton as determined by the electron and muon reconstruction algorithms. Medium leptons are required to have $p_T^{\text{lep,cone}} > 10\,\text{GeV}$ and the jet nearest to the lepton should fail the medium b tagging working point. Medium electrons are further required to satisfy criteria similar to the ones applied at the trigger level. The requirements are: the width of the electron cluster in η-direction $\sigma_{i\eta i\eta} < 0.011(0.030)$ when $|\eta| \leq 1.479$ ($|\eta| > 1.479$); the ratio of energy associated to the electron in the HCAL to the energy in the ECAL $H/E < 0.10$; the difference between the reciprocal of the electron cluster energy and the reciprocal of its track momentum $(1/E - 1/p) > -0.04$; medium electron tracks are not allowed to miss any hits in inner pixel detector and to not originate from a photon conversion. Finally, only medium electrons not overlapping with medium muons within $\Delta R < 0.4$ are considered.

The tight lepton selection is used to select events in the signal region (SR). For this purpose, a lepton identification algorithm based on boosted decision trees is used, discriminating the prompt leptons from nonprompt and misidentified ones. Thereafter this will be referred to as the prompt-lepton MVA. The MVA is trained separately for electrons and muons [72]. Several observables related to the lepton are used as input variables such as the p_T^{lep}, η^{lep}, relative isolation $I^{\text{lep}}/p_T^{\text{lep}}$, $|d_{xy}|$, and $|d_z|$. The jet reconstruction and b tagging algorithms are applied to

the charged and neutral particles reconstructed in a cone around the lepton direction. The ratio of the lepton p_{T} to the reconstructed jet p_{T} and the component of the lepton momentum in a direction perpendicular to the jet direction are also used as inputs to the MVA. Tight leptons are required to have prompt-lepton MVA score greater than 0.5 (0.3) for muons (electrons). Muons are additionally required to pass the medium PF muon identification criteria as described in Ref. [69]. Contrary to medium leptons, the p_{T} of tight leptons is not replaced by the $p_{\mathrm{T}}^{\mathrm{cone}}$ as these leptons are likely to be prompt.

4.5 Missing transverse momentum

The missing transverse momentum vector $\vec{p}_{\mathrm{T}}^{\,\mathrm{miss}}$ is computed as the negative vector sum of the transverse momenta of all the PF candidates in an event and its magnitude is denoted as $p_{\mathrm{T}}^{\mathrm{miss}}$ [73]. The $p_{\mathrm{T}}^{\mathrm{miss}}$ is modified to account for corrections to the energy scale of the reconstructed jets in the event.

The variable $H_{\mathrm{T}}^{\mathrm{miss}}$ is defined in the same way as $p_{\mathrm{T}}^{\mathrm{miss}}$, but considering only jets that fulfill the criteria described in Sections 4.2 and 4.3, as well as electrons and muons passing the medium selection criteria, when evaluating the p_{T} sum. The observable $H_{\mathrm{T}}^{\mathrm{miss}}$ has the advantage of being less sensitive to pileup, as soft hadrons that predominantly originate from pileup do not enter its computation, and can therefore be used as a complement to $p_{\mathrm{T}}^{\mathrm{miss}}$ in a MVA algorithm.

This analysis also uses a linear combination, also referred to as a linear discriminant (LD), of $p_{\mathrm{T}}^{\mathrm{miss}}$ and $H_{\mathrm{T}}^{\mathrm{miss}}$ defined as $p_{\mathrm{T,LD}}^{\mathrm{miss}} = 0.6p_{\mathrm{T}}^{\mathrm{miss}} + 0.4H_{\mathrm{T}}^{\mathrm{miss}}$ [72]. The two observables are less correlated for events in which the $p_{\mathrm{T}}^{\mathrm{miss}}$ arises from artificial effects compared to events with genuine $p_{\mathrm{T}}^{\mathrm{miss}}$. The jet energy corrections are propagated to $H_{\mathrm{T}}^{\mathrm{miss}}$ and $p_{\mathrm{T,LD}}^{\mathrm{miss}}$.

5 Event selection

The signature of the $\mathrm{b\bar{b}W^+W^-}$ signal is characterised by the decay of each of the Higgs bosons, $\mathrm{H} \to \mathrm{b\bar{b}}$ and $\mathrm{H} \to \mathrm{W^+W^-}$. The $\mathrm{H} \to \mathrm{b\bar{b}}$ decay can be identified by the two jets originating from the hadronisation of each of the b quarks. In order to identify $\mathrm{H} \to \mathrm{b\bar{b}}$ candidates, events are required to have at least one b-tagged small-radius jet, accounting this way for inefficiencies in b tagging. In case the Higgs boson is highly Lorentz-boosted, the two b jets from the $\mathrm{H} \to \mathrm{b\bar{b}}$ decay are merged and they are reconstructed one single large-radius jet. Events are selected when they have one large-radius jet with least one of the subjets b-tagged.

The VBF jet candidates must not overlap with the $\mathrm{H} \to \mathrm{b\bar{b}}$ candidates, either the small-radius jets within $\Delta R < 0.8$, or the large-radius jet within $\Delta R < 1.2$. Additionally, only pairs of jets with invariant mass $m_{jj} > 500\,\mathrm{GeV}$ and separation $\Delta\eta_{jj} > 3$ are considered. The leading pair in invariant mass determines the two VBF jets considered.

The two channels of this analysis are characterised by the decay products of the $\mathrm{H} \to \mathrm{W^+W^-}$ decay. The "single-lepton" channel targets events where only one W boson decays leptonically, while the "dilepton channel" targets events where both W bosons do.

The first two steps of the event selection are the event preselection and trigger selection. The selected events are then evaluated using DNNs and categorised as described in Section 6.

5.1 Event preselection

Events containing a pair of leptons passing the loose selection and with an invariant mass less than 12 GeV are rejected as they are likely to originate from quarkonia decays. Events with a pair of loose-selection leptons, with opposite electric charge but same flavour, within 10 GeV

of the mass of the Z boson (of 91.2 GeV [74]), are vetoed to remove DY and $t\bar{t}Z$ backgrounds. To suppress effects related to beam halo, detector noise, etc., the primary vertex in all events is required to have longitudinal distance from the collision point $|z_{vtx}|$ less than 24 cm, radial distance $|r|$ less than 2 cm, and at least four associated tracks.

5.2 Trigger selection

The events selected in the single-lepton channel are required to pass either the single-electron or the single-muon trigger, based on the offline-reconstructed lepton flavour, selected as described in Section 4.4. The p_T requirements applied in this analysis (Section 5.3) are chosen to be close to the trigger threshold (22–35 GeV) to reduce turn-on effects in the trigger selection efficiency. Residual turn-on effects are corrected for the simulated events using scale factors and corresponding systematic uncertainties. In the dilepton channel, the acceptance for the HH signal is increased by using a combination of single-lepton and dilepton triggers. The dilepton triggers have a lower p_T threshold for the leading-p_T lepton (17–23 GeV) compared to the single-lepton triggers, which allows lowering the p_T thresholds for the electrons and muons reconstructed offline.

5.3 Single-lepton channel

Events in the single-lepton channel are required to contain a lepton satisfying tight selection criteria with $p_T > 32$ GeV for an electron and 25 GeV for a muon. Events containing a second lepton passing the tight selection criteria are vetoed to avoid overlap with the dilepton channel.

Events selected in the single-lepton channel are required to contain either at least three small-radius jets (Section 4.2) or at least one large-radius jet (Section 4.3) and at least one small-radius jet, which is separated from the large-radius jet by $\Delta R > 1.2$. At least one of the three small-radius jets, or in the latter case the large-radius jet, is required to be b-tagged. Overlap with the events selected by the $HH \to \tau\tau b\bar{b}$ search is removed by vetoing events containing at least one hadronically decaying tau lepton, identified by the DEEPTAU algorithm [75] as described in Ref. [76].

5.4 Dilepton channel

Events selected in the dilepton channel must contain two leptons that pass the tight selection criteria and have opposite electric charges. The leading lepton is required to have $p_T > 25$ GeV and the subleading one $p_T > 15$ GeV. Events containing a third lepton passing the tight selection criteria are vetoed, to avoid overlap with the search for $HH \to ZZb\bar{b}$ with four charged leptons in the final state. The events are further required to contain at least either one b-tagged large-radius jet or one b-tagged small-radius jet.

6 Analysis strategy

Events passing the single-lepton and dilepton selections are separated in different categories based on the signal purity, utilizing the $H \to b\bar{b}$ signal topology and fully connected DNN multiclassifiers, as described later in this section. The event categorisation is summarised in Tables 1 and 2. To extract the HH signal we perform a maximum likelihood fit in the asymptotic approximation [77] on the distribution of the DNN score, using the modified frequentist CL_s method [23, 24], simultaneously on the signal and background event categories. To account for the effects of the systematic uncertainties, we include them as nuisance parameters (Section 8) in the maximum likelihood fit.

Four DNNs are trained separately for the single-lepton and dilepton channels, and for the resonant and nonresonant signals. The DNNs for the nonresonant signal are trained on all available simulated signal events representing different coupling scenarios. For the resonant signal the DNNs are trained on all signal samples and the networks are parametrised [78] according to the mass of the resonance decaying to the two Higgs bosons, which is provided in the training inputs for signal events and random values for background events in the same proportions. The background events are drawn from the simulated samples described in Section 3.2.

The DNN architecture is complemented by a Lorentz Boost Network [79] acting as input preprocessor. This network takes as input the four-vectors of the reconstructed particles and creates additional observables (such as a two-particle invariant mass or angle difference in their centre-of-mass), which are then given as input to the DNN together with other variables related to the HH signal topology. The combined Lorentz Boost Network and following dense networks are trained all together.

Two of the variables used as input to the DNN for each channel are shown in Fig. 4. The distributions are shown after performing a maximum likelihood fit on the data in the distribution of the variable displayed, using the same set of nuisance parameters (Section 8) as in the likelihood fit used to extract the signal. The variables are from upper left to lower right: the H_{T} variable, defined as the scalar sum of all selected small-radius jets p_{T}; the invariant mass of the two b-tagged jets after the regression correction (Section 4.2); the invariant mass of the two leptons; the $p_{\mathrm{T,LD}}^{\mathrm{miss}}$ as defined in Section 4.5. The highest ranking variable in terms of discrimination power is the H_{T} for both single-lepton and dilepton channels. The invariant mass of the two b-tagged jets and the invariant mass of the two leptons are the second highest ranking variables for the two channels, respectively. The $p_{\mathrm{T,LD}}^{\mathrm{miss}}$ ranks fifth for the dilepton channel, after the information about the flavour of the two leptons.

The DNNs are trained as multiclassifiers, which means that they learn each physics process ($\mathrm{t\bar{t}}$, DY, etc.) separately, which in the machine learning context are referred to as "classes". The multiclassifier assigns a score between $[0, 1]$ for each class to each event. This score is related to the probability of an event belonging to the corresponding class. The event categorisation into background and signal categories is based on the DNN output scores; each event is assigned to the class with the highest probability. In the SM nonresonant case there are two signal categories as defined by the DNN, ggF and VBF. In the resonant search and the anomalous couplings interpretation only the ggF process is considered, therefore there is only one signal category. To form the background categories, the DNN classes for minor background processes are grouped together with a major background with a similar topology, in order to simplify the fitting process and reduce the statistical uncertainties. In the dilepton channel, multiboson events are categorised together with the DY events to form the "DY + Multiboson" category, while single top quark, $\mathrm{t\bar{t}Z}$, SM single Higgs boson processes and others are included in the same category as the dominant $\mathrm{t\bar{t}}$ background forming the "Top + Other" category. In the single-lepton channel, single top quark and SM single Higgs boson processes are included in the same event category as the dominant $\mathrm{t\bar{t}}$ background, "Top + Higgs" category, while all other processes are included in the same category as the W+jets background, "W+jets + Other".

The signal categories are further divided into subcategories according to the b jet topology and multiplicity. Events with one large-radius jet, as defined in Section 4.3, are considered in the boosted category if they are b-tagged. If there are large-radius jets that are not b-tagged or if there is no large-radius jet at all, the events are divided according to the number of small-radius jets into events with exactly 1 b-tagged jet and events with at least 2 b-tagged jets. Remaining

Table 1: Summary of the categories of events according to the DNN-based multiclassification and $H \to b\bar{b}$ topology for the single-lepton channel. The VBF category is considered only in the nonresonant search.

Single-lepton channel			
Categories	Subcategories		
HH (ggF)	Resolved 1b	Resolved 2b	Boosted
HH (VBF)	Resolved 1b	Resolved 2b	Boosted
Top + Higgs	Resolved		Boosted
W+jets + Other	Inclusive		

Table 2: Summary of the categories of events according to the DNN-based multiclassification and $H \to b\bar{b}$ topology for the dilepton channel. The VBF category is considered only in the nonresonant search.

Dilepton channel			
Categories	Subcategories		
HH (ggF)	Resolved 1b	Resolved 2b	Boosted
HH (VBF)	Resolved 1b	Resolved 2b	Boosted
Top + Other	Resolved		Boosted
DY + Multiboson	Inclusive		

events without any b-tagged jet will be considered for the data-driven estimation of the DY background, as described in Section 7.2. The categories for each decay channel are summarised in Tables 1 and 2. The total number of categories in both dilepton and single-lepton channels is nine for the nonresonant interpretations and six for the resonant, as we only consider ggF for the latter.

The discriminants used in the maximum likelihood fit for signal extraction are the DNN output scores for each category and channel, combined into a single likelihood function, and are shown in Figs. 5, 6, 7, and 8. The binning for the signal categories is performed using quantile binning such that the signal response is flat, while the reverse is done for the background categories. The optimisation of the binning was done separately for each data taking year, while the figures contain all the data. Therefore for illustration purposes the binning shown might have slight differences to what was used in the signal extraction and the signal response may not appear flat. One exception is the resonant search in the dilepton channel in which the DNN score of the signal categories is split in bins of the Heavy Mass Estimator (HME) [80] as shown in Fig. 8. This variable estimates the most likely invariant mass of the heavy resonance, considering the two neutrinos from the W bosons leptonic decays in the final state. In this case, the maximum likelihood fit is performed on the two-dimensional (2D) distribution of the DNN output score and the HME.

7 Background estimation

The shape of the $t\bar{t}$ contribution for both channels is estimated using simulated events. The $t\bar{t}$ and single top quark normalisations are determined by the maximum likelihood fit, and they are constrained by the "Top+Higgs" or "Top+Other" event category, depending on the channel. The same procedure is used for the W+jets background in the single-lepton channel. To estimate the background contribution of jets misidentified as leptons and, in the dilepton channel, the DY background contribution, control samples in data are used. The rest of the

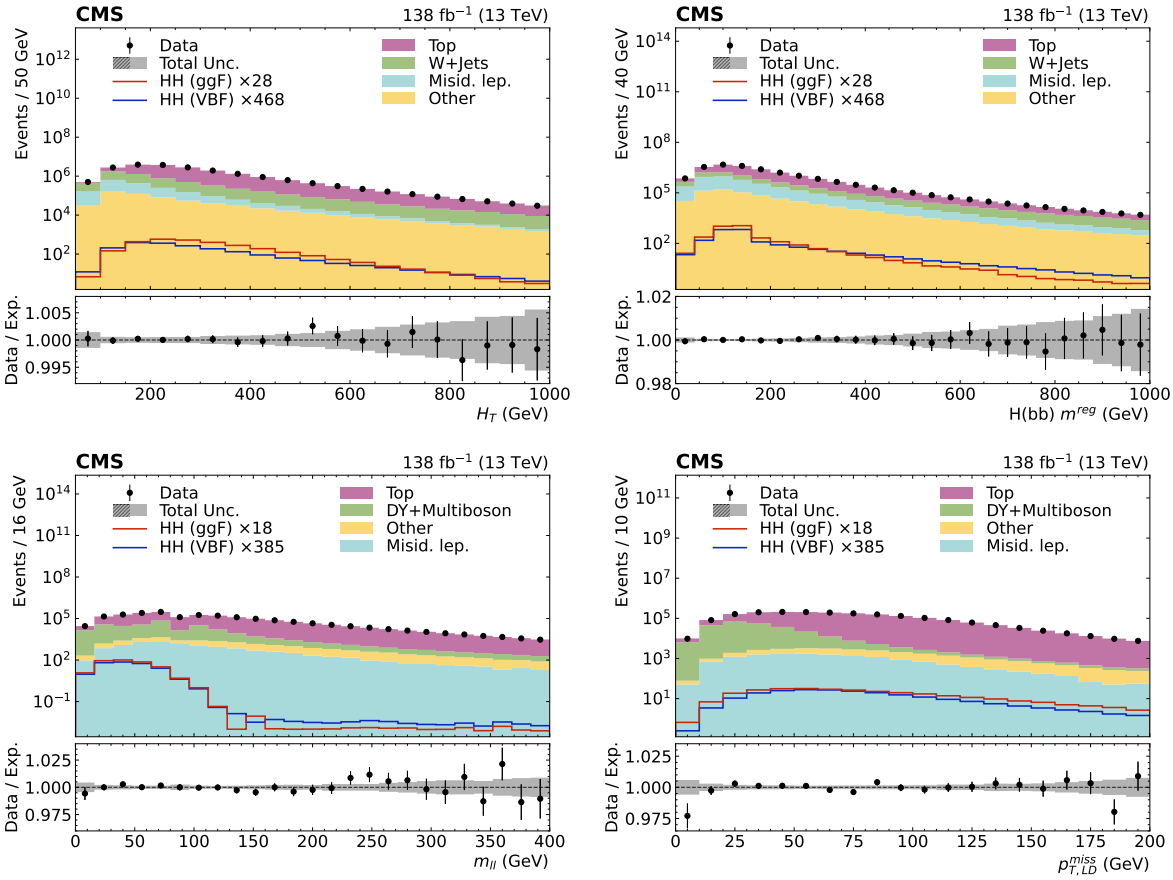

Figure 4: The distributions of some of the discriminants included in the DNN training for the single-lepton channel (upper) and the dilepton channel (lower). The distributions are shown after performing a maximum likelihood fit on the data for the variable pictured, using the same set of nuisance parameters (Section 8) as in the likelihood fit used to extract signal. The variables are from upper left to lower right: the H_{T} variable, defined as the scalar sum of all selected jets p_{T}; the invariant mass of the two b-tagged jets; the invariant mass of the two leptons; the $p_{\mathrm{T,LD}}^{\mathrm{miss}}$, as defined in Section 4.5. The signal shown is scaled to the observed upper limit on its cross section.

backgrounds are estimated using simulated events.

7.1 Estimation of the misidentified-lepton background

The background arising from events with misidentified leptons is estimated using the "fake-factor" method in Refs. [72] and [81]. A sample of events is selected by requiring that all lepton criteria of Section 5 must be satisfied, with the exception that at least one electron or muon passes the medium and fails the tight selection (with p_{T} requirements replaced by the same ones on $p_{\mathrm{T}}^{\mathrm{cone}}$), preventing overlap with the signal region.

An estimate of the misidentified-lepton background in the signal region is obtained by applying suitably chosen weights to these events. The weights, denoted by the symbol w, are given by the expression:

$$w = (-1)^{n+1} \prod_{i=1}^{n} \frac{f_i}{1 - f_i}, \tag{2}$$

where f_i denotes the probability for an electron or a muon that passes the medium selection to

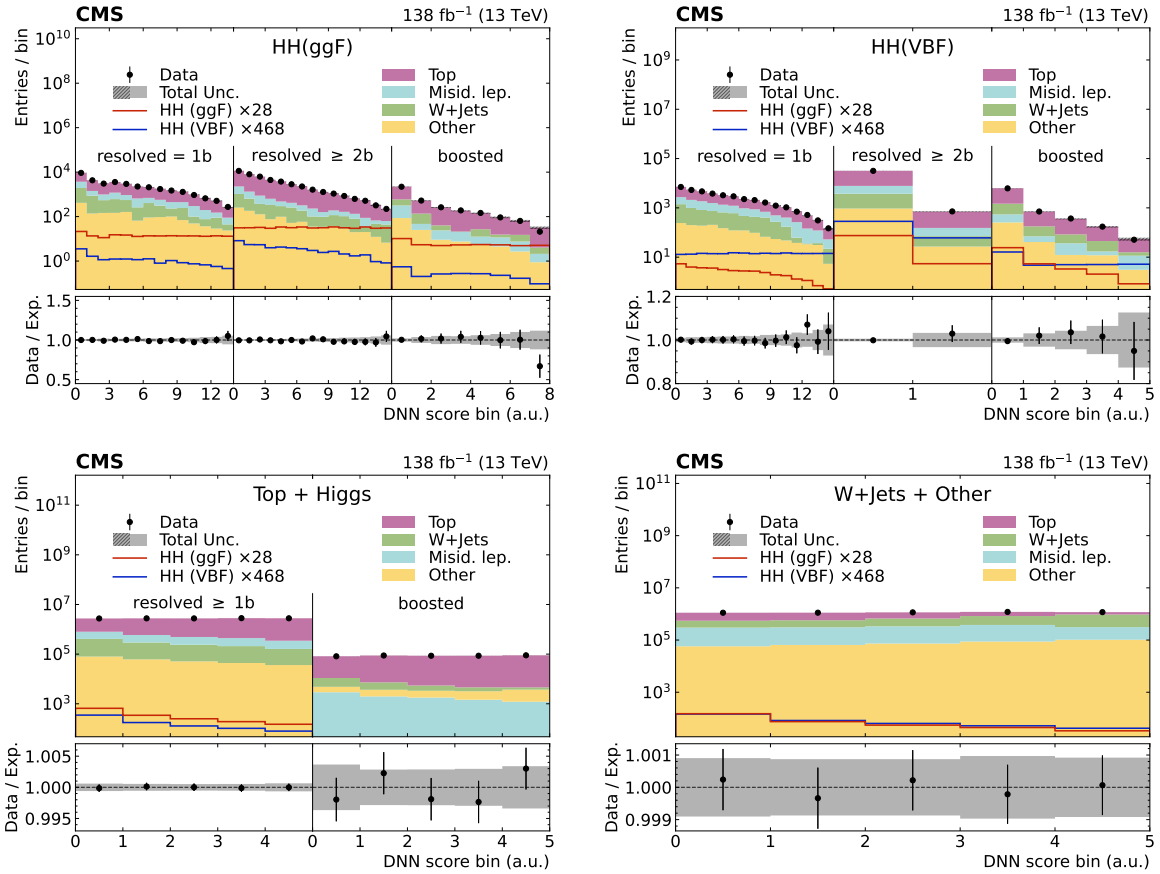

Figure 5: The distributions of the DNN discriminants of the nonresonant search for each event category for the single-lepton channel, after performing a maximum likelihood fit to the same distributions in data. The DNN discriminant for the HH (ggF) category is shown on the upper left, HH (VBF) on the upper right, Top+Higgs on the lower left and W+jets + Other on the lower right. The event categories are summarised in Table 1. The signal shown is scaled to the observed upper limit on its cross section.

also satisfy the tight selection. The probabilities f_i are measured separately for electrons and muons, as described in Ref. [72] in a control region dominated by the multijet background.

The product extends over the number of electrons and muons that pass the medium and fail the tight selection (n). In case an event of the single-lepton (dilepton) channel contains more than one (two) medium leptons, only the leading (and subleading) lepton in $p_{\mathrm{T}}^{\mathrm{cone}}$ is considered when computing the weights according to Eq. (2), and thus $n = 1$ ($n = 1$ or 2) in the single-lepton (dilepton) channel. For $n = 2$ the weights become negative to avoid double counting. The contributions of other backgrounds are subtracted based on the expectation from simulation.

7.2 Estimation of the Drell–Yan background

The DY background in the dilepton channel is estimated using data events that pass the nominal event selection but have no reconstructed b-tagged jets. This "0 b tag region" is found to be dominated by DY events. We create additional DY enriched regions by inverting the selection requirement on the dilepton mass targeting DY events. This inverse selection is applied for events with 0, 1 and 2 b-tagged jets. Using events with dilepton mass within 10 GeV from the Z boson mass, we calculate transfer weights from the 0 b tag region to the 1 and 2 b tag categories.

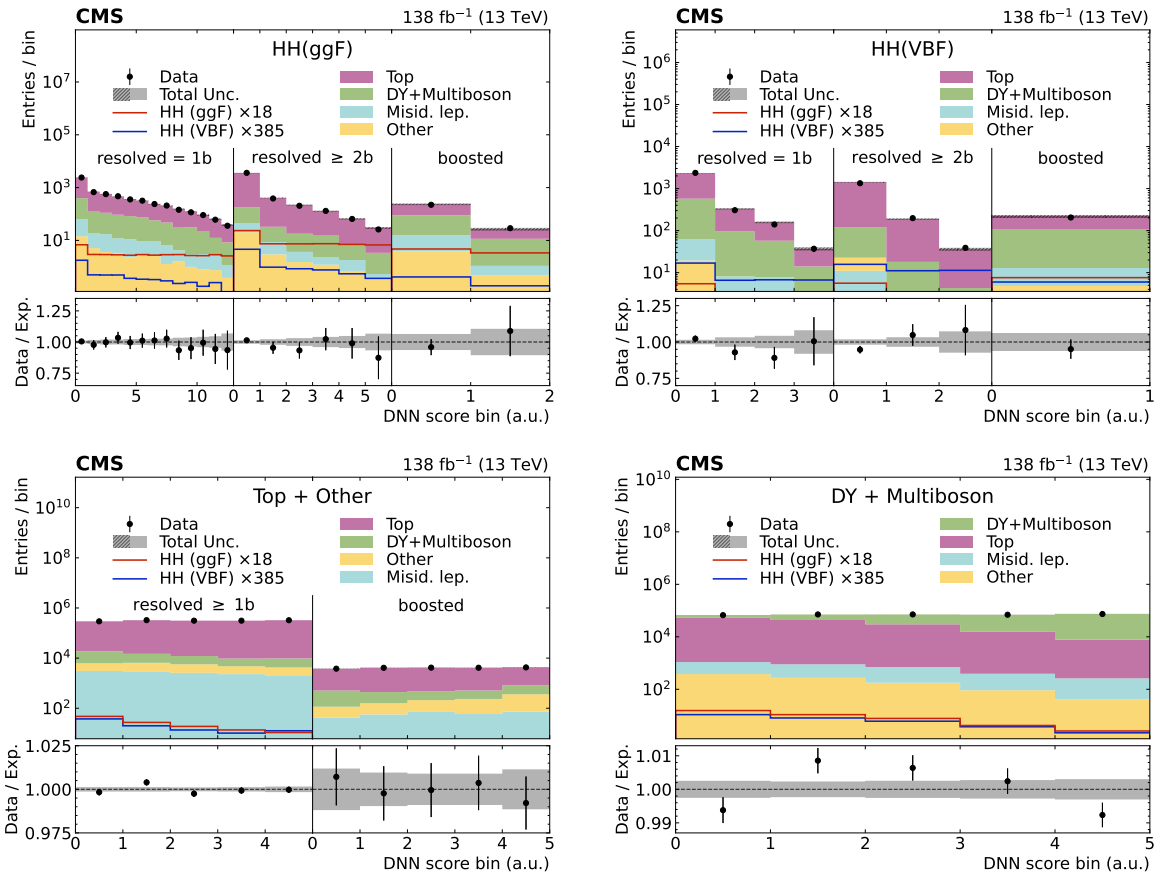

Figure 6: The distributions of the DNN discriminants of the nonresonant search for each event category for the dilepton channel, after performing a maximum likelihood fit to the same distributions in data. The DNN discriminant for the HH (ggF) category is shown on the upper left, HH (VBF) on the upper right, Top+Other on the lower left and DY+Multiboson on the lower right. The event categories are summarised in Table 2. The signal shown is scaled to the observed upper limit on its cross section.

In the signal region, these weights are applied to the 0 b tag region using two orthogonal sets of events to estimate the DY in the 1 and 2 b tag regions, in order to avoid bias from using the same events twice. The same process is applied to the boosted categories. The weights are found to be independent of the lepton flavour, and the proportion of DY events in the eμ channel from tau lepton decays to e or μ is insignificant. Therefore we calculate the weights in ee and $\mu\mu$ events simultaneously and apply them to the ee, $\mu\mu$ and eμ events. When extracting the shape of the DY distribution in the 0 b tag region from the data, the contribution from other background sources is estimated using simulated events.

8 Systematic uncertainties

Systematic uncertainties are introduced as nuisance parameters in the maximum likelihood fit used to extract the signal.

A number of systematic uncertainties are considered that affect the yield and the shapes of the HH signal and the background processes. Theoretical uncertainties in the strong interaction coupling α_s, and parton distribution function shapes that affect the cross section of all the simulated processes are included.

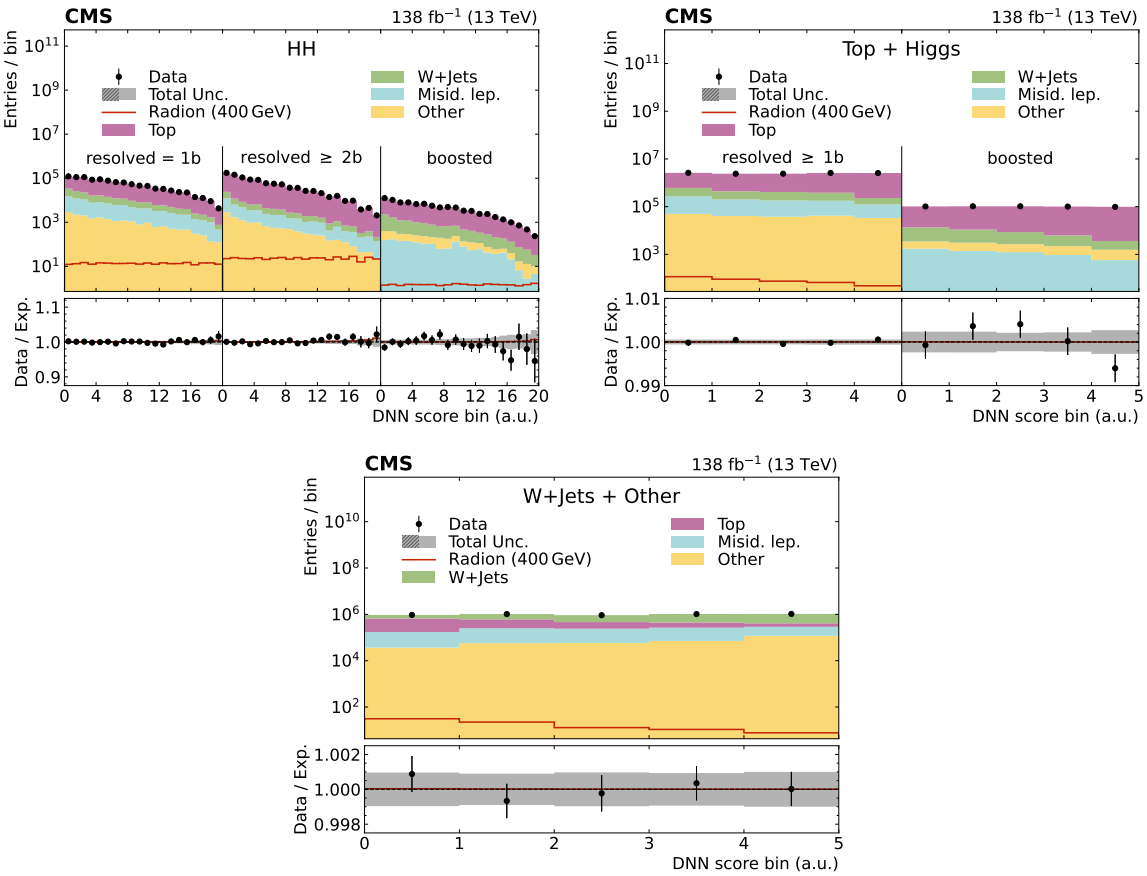

Figure 7: The distributions of the DNN discriminants of the resonant search for each event category for the single-lepton channel, after performing a maximum likelihood fit to the same distributions in data. The DNN shown corresponds to a scalar resonance with mass 400 GeV. The DNN discriminant for the HH (ggF) category is shown on the upper left, Top+Higgs on the upper right and W+jets + Other on the lower. The event categories are summarised in Table 1. The signal shown is scaled to a cross section of 1 pb.

Theoretical uncertainties in the nonresonant HH cross section via ggF are applied as a function of κ_λ and include renormalisation and factorisation scale uncertainties, including the mass scale of the top quark [10]. In the SM this uncertainty amounts to $+6\%/-26\%$. An additional factor of $\pm 3.0\%$ is applied to account for PDF+α_s uncertainties. The uncertainties on the VBF production cross section include a $+0.03/-0.04\%$ (scale) and a $\pm 2.1\%$ (PDF+α_s) [82, 83] uncertainties. All uncertainties on the signal cross section are only applied when quoting limits relative to the theoretically predicted cross section. An additional 10% normalisation uncertainty is applied to the VBF, related to the colour correlated recoil scheme [84] used in PYTHIA. It is estimated by comparing the nominal simulated samples produced with the default global recoil scheme to samples simulated with the dipole-recoil scheme.

The uncertainty in the top quark mass value assumed in the simulations of the $\mathrm{t\bar{t}}$ background is derived by varying the mass value by $-2.7/+2.8\%$ [85]. Theoretical uncertainties on the branching fractions [86] of H decays are applied to HH signal and single Higgs boson background ($\mathrm{H} \to \mathrm{b\bar{b}}$, $\mathrm{H} \to \mathrm{WW}$ and $\mathrm{H} \to \tau\tau$ branching fractions, $+1.24/-1.26\%$, $+1.53/-1.52\%$, and $+1.65/-1.63\%$ respectively).

Other theory uncertainties include electroweak corrections for the $\mathrm{t\bar{t}Z}$ ($+0.0/-0.2\%$) and $\mathrm{t\bar{t}W}$

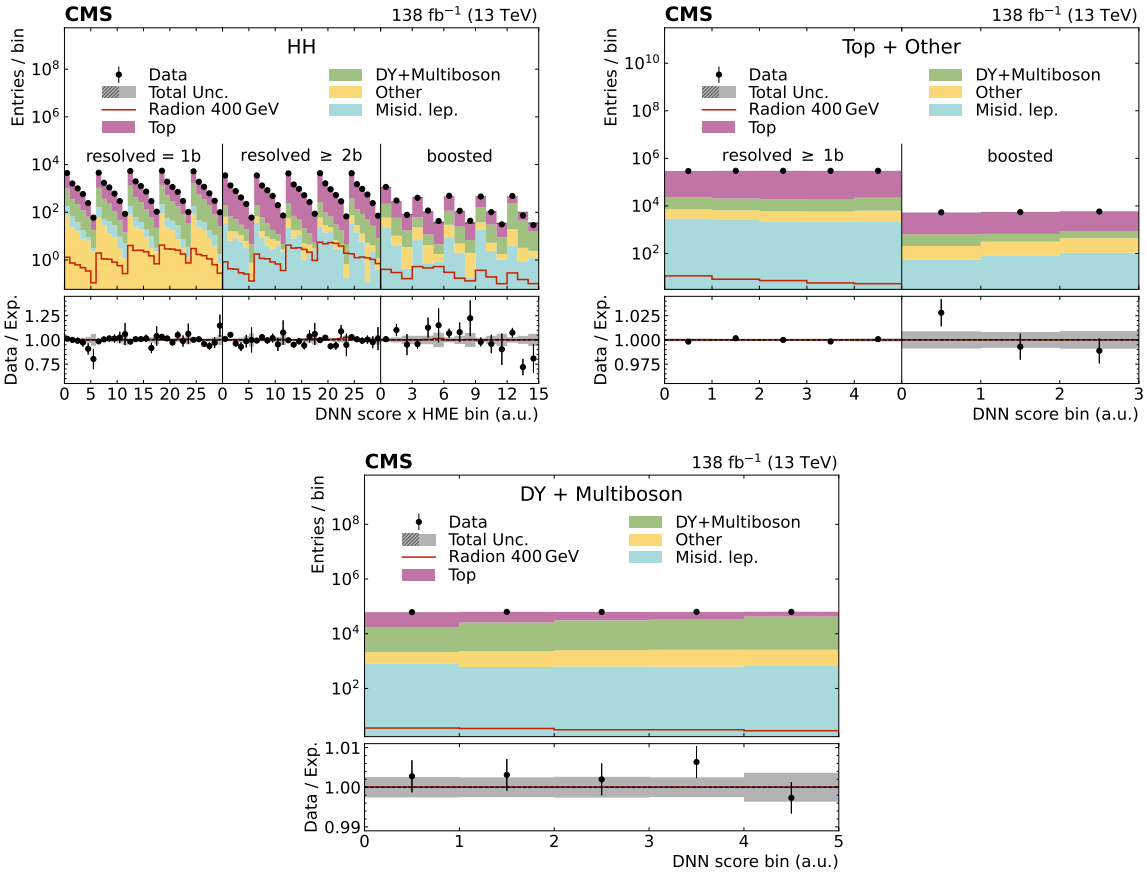

Figure 8: The distributions of the DNN discriminants of the resonant search for each event category for the dilepton channel, after performing a maximum likelihood fit to the same distributions in data. The DNN shown corresponds to a scalar resonance with mass 400 GeV. The DNN discriminant for the HH (ggF) category divided in bins of HME is shown on the upper left, Top+Other upper right and DY+Multiboson on the lower. The event categories are summarised in Table 2. The signal shown is scaled to a cross section of 1 pb.

($+0.0/-3.2\%$) processes as well as PDF weights ($\pm 4.2\%$ for $\mathrm{t\bar{t}}$, $\pm 1.2\%$ for single top quark, $\pm 4.6\%$ for VV, $\pm 2.8\%$ for $\mathrm{t\bar{t}Z}$, and $\pm 2\%$ for $\mathrm{t\bar{t}W}$). Parton shower acceptance uncertainties are applied as shape variations for all background processes.

A shape uncertainty that corresponds to the NNLO correction of the top quark p_{T} is applied to the $\mathrm{t\bar{t}}$ simulated samples. The relative uncertainty is 100%, i.e. an uncertainty as large as the correction is applied to the simulated $\mathrm{t\bar{t}}$ events.

The integrated luminosities for the 2016–2018 data taking years separately have 1.2–2.5% individual uncertainties [20–22], while the overall uncertainty for the 2016–2018 period is 1.6%.

During the 2016–2017 data taking, a gradual shift in the timing of the inputs of the ECAL Level-1 trigger in the region at $|\eta| > 2.0$ caused a specific trigger inefficiency. For events containing an electron or a jet with $p_{\mathrm{T}} > 50\,\mathrm{GeV}$ or 100 GeV respectively, in the region $2.5 < |\eta| < 3.0$ the efficiency loss is 10–20%, depending on p_{T}, η, and data taking period. Correction factors are computed from data and applied to the acceptance evaluated from simulation. In addition, a normalisation uncertainty is included in the statistical fit.

A shape uncertainty related to the pileup in simulation and its 5% [87] inelastic pp cross section uncertainty is applied to all simulated samples.

The trigger selection efficiency is corrected to account for differences between data and simulation. The uncertainties in these corrections applied to simulated samples constitute a shape uncertainty. Similarly, the muon and electron identification efficiencies are also corrected and corresponding shape uncertainties are introduced.

An uncertainty in the efficiency of the selection rejecting jets originating from pileup, as well as uncertainties on jet energy scale and resolution, are used as shape uncertainties for all simulated samples.

Corrections based on the area and energy density of the jet are applied in order to compensate for pileup effects. Nuisance parameters that affect the shape related to the identification of the jet flavour are also included. Different types of jet flavour contamination are treated with separate parameters.

A set of systematic uncertainties is included in the fit regarding the estimation of the misidentified-lepton background from control samples in data, as well as the DY background. The uncertainties regarding the backgrounds derived from data are assigned and validated using simulated events through closure tests on the DNN distributions entering the fit to ensure that they cover the observed amount of nonclosure. For the misidentified-lepton background estimation, they are shape uncertainties in the single-lepton channel and normalisation uncertainties in the dilepton channel. The DY estimation closure uncertainty, applicable only to the dilepton channel, is a shape uncertainty for all background categories and a normalisation uncertainty for the HH signal categories.

9 Results

For each signal model considered, a profile binned likelihood fit [23, 24, 88] is performed to the distributions of the DNN discriminants for each event category (Figs. 5 to 8) simultaneously. For the SM-like signal search the fit includes 18 categories while 12 categories are used for the resonant search and the anomalous couplings interpretation. The categories dominated by background events allow for in-situ constraints on the main background processes. There are three background-dominated categories for the single-lepton channel and three for the dilepton

channel. No significant excess over the background-only hypothesis is observed. Upper limits are set on nonresonant and resonant Higgs boson pair production at 95% CL using the modified frequentist CL_s method in the asymptotic approximation.

The observed (expected) upper limit on the inclusive $pp \to HH$ cross section is 14 (18) times the value expected by the SM (Fig. 9). The observed (expected) limit on the HH production via VBF is 277 (301) times the SM value and is shown in Fig. 10. In this case the SM value is assumed for the ggF HH process. Figs. 9 and 10 show the contributions from individual channels as well.

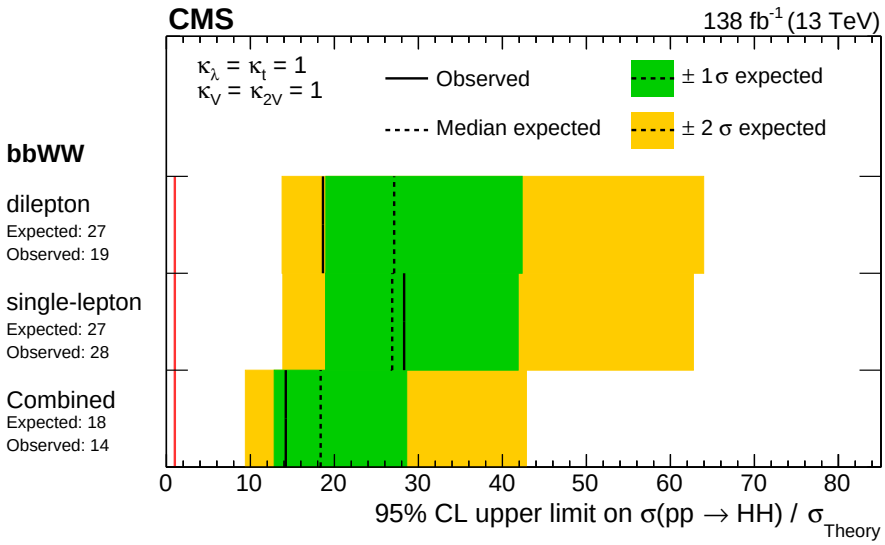

Figure 9: Observed and expected 95% CL upper limits on the inclusive nonresonant HH production cross section divided by the SM prediction obtained for both single-lepton and dilepton channels, and from their combination. The green and yellow bands show the 1 and 2σ confidence intervals, corresponding to 68 and 95% CL, while the red line shows the SM prediction.

Figures 11 and 12 show the limits on the inclusive and the VBF production cross section as a function of κ_λ and κ_{2V} modifiers, respectively, assuming standard model values for all other couplings. The κ_λ modifier is constrained between $[-7.2, 13.8]$ (expected $[-8.7, 15.2]$). The κ_{2V} modifier is constrained between $[-1.1, 3.2]$ (expected $[-1.4, 3.5]$). The latter result has similar sensitivity to the $\gamma\gamma b\bar{b}$ channel which constrained the κ_{2V} modifier in the range $[-1.3, 3.5]$ (expected $[-0.9, 3.1]$) [89].

The exclusion contours on the κ_λ and κ_{2V}, κ_V and κ_{2V}, κ_t and κ_λ are shown in Figs. 13, 14, and 15, respectively, while all other Higgs boson couplings are set to the values predicted by the SM.

As explained in Section 3.1, we can study modified HH couplings as well as anomalous couplings which are not predicted in the SM. The set of coupling modifiers studied is κ_λ, κ_t, c_2, c_g and c_{2g} (Figs. 1 and 3), based on an effective field theory parameterisation. Two sets of benchmarks referred to as "JHEP04(2016)01" [90] and "JHEP03(2020)91" [91] have been proposed, which are different combinations of (κ_λ, κ_t, c_2, c_g, c_{2g}). The results are interpreted as limits on the ggF production cross section for each of the benchmarks considered, shown in Fig. 16. In addition, a limit scan for the c_2 coupling is shown in Fig. 17. The c_2 coupling is constrained between $[-0.8,\ 1.3]$ (expected $[-1.0, 1.4]$) at 95% CL. Exclusion limits contours are drawn in the κ_λ-c_2 plane, shown in Fig. 18. All other Higgs boson couplings are set to the values predicted by the SM.

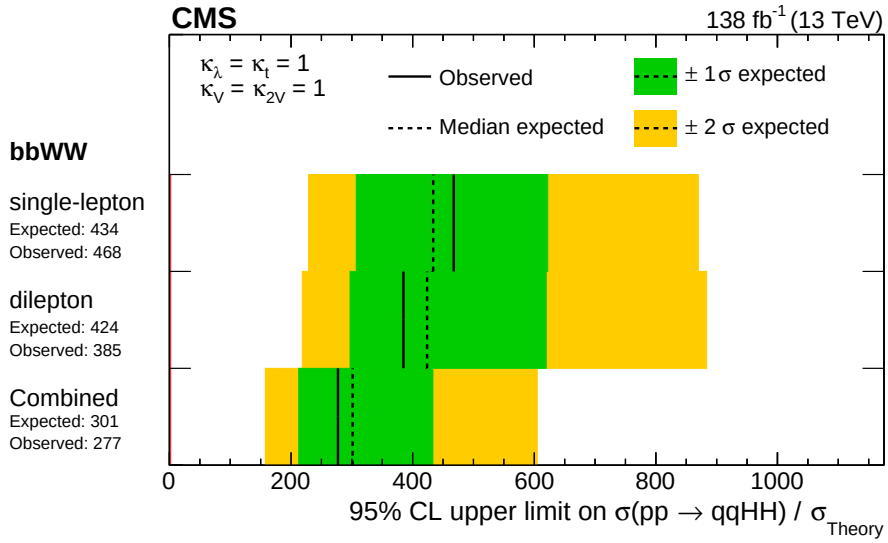

Figure 10: Observed and expected 95% CL upper limits on the nonresonant HH production via vector boson fusion cross section divided by the SM prediction obtained for both single-lepton and dilepton channels, and from their combination. The green and yellow bands show the 1 and 2σ confidence intervals, corresponding to 68 and 95% CL, while the red line shows the SM prediction.

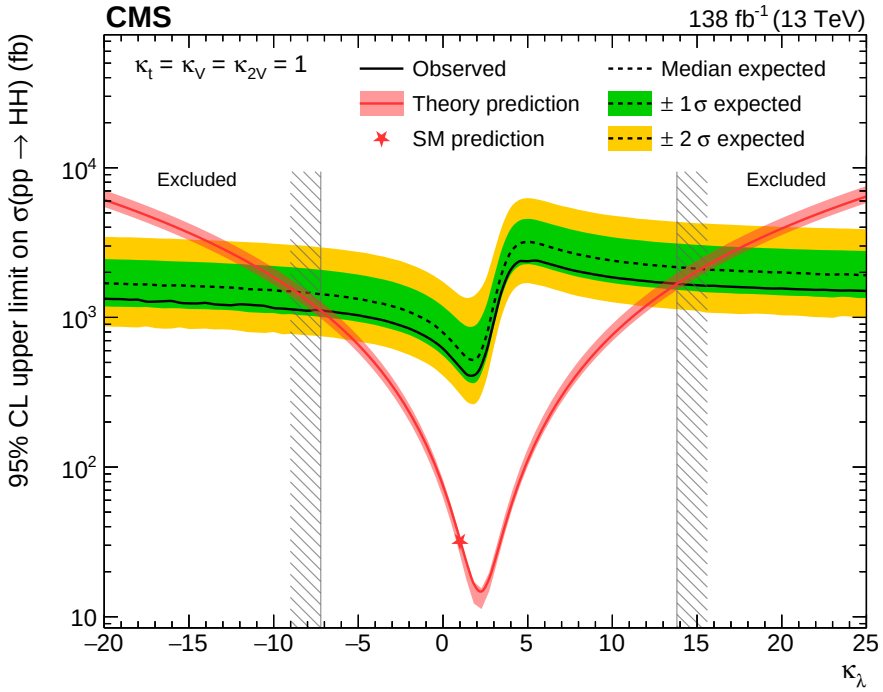

Figure 11: Observed and expected 95% CL upper limits on the nonresonant HH production cross section as a function of the Higgs boson self-coupling strength modifier κ_λ. The green and yellow bands show the 1 and 2σ confidence intervals, corresponding to 68 and 95% CL. All Higgs boson couplings other than λ are set to the values predicted by the SM. Overlaid in red is the curve representing the predicted HH production cross section.

The results of the resonant search are extracted using the same strategy and similar categories to the nonresonant one. The limits are presented as a function of the heavy resonance mass hypothesis in the range between 250 and 900 GeV, since 250 GeV is the threshold for on-shell

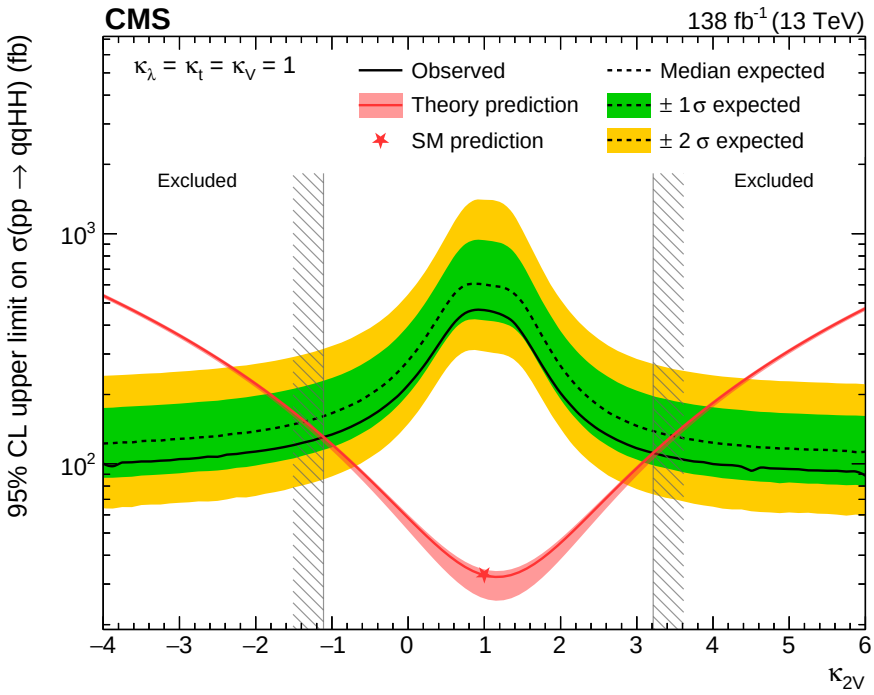

Figure 12: Observed and expected 95% CL upper limits on the nonresonant HH production via VBF cross section as a function of the effective coupling κ_{2V}. The green and yellow bands show the 1 and 2σ confidence intervals, corresponding to 68 and 95% CL. The ggF contribution in this case is set to the SM expectation. All other Higgs boson couplings are set to the values predicted by the SM. Overlaid in red is the curve representing the predicted HH production cross section.

HH production. Beyond 900 GeV the topology of the Higgs boson decays becomes predominantly highly boosted and the analysis presented in this paper is not optimal. A previously published CMS search covers this phase-space [92]. The resonances are assumed to have a narrow width, i.e. width smaller than the experimental resolution for the reconstructed Higgs boson mass which is 10–15%. Figure 19 shows the limits for the spin-0 and spin-2 signal hypotheses. For the spin-0 (2) scenario the limits on the cross section vary between 5540 (6368) and 20 (15) fb corresponding to the 250 GeV and 900 GeV mass points, respectively. For resonant mass above 700 GeV the limits set by the $\mathrm{b\bar{b}W^+W^-}$ search are comparable to those by the $\gamma\gamma\mathrm{b\bar{b}}$ search [93]. Theoretical predictions for the spin-0 radion and the spin-2 graviton are shown against the respective exclusion limits. The parameters Λ and $\tilde{\kappa} = \kappa/M_{\mathrm{Pl}}$ correspond to the energy scale and warp factor of the so-called "bulk" benchmark of the warped extra dimensions scenarios [94, 95], where M_{Pl} is the Planck mass. The values of these parameters have been chosen based on the current constraints from other measurements. While these are representative models for this type of search, the search is performed in a model-independent way, only depending on the resonance mass, width, and spin.

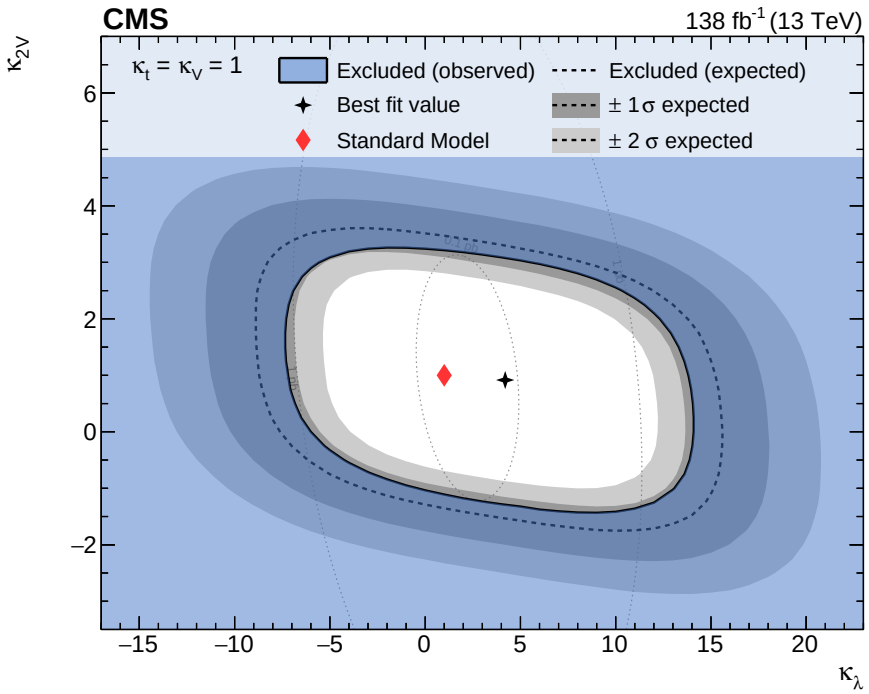

Figure 13: Observed and expected 95% CL exclusion limits on the nonresonant HH production cross section as a function of the effective couplings κ_λ and κ_{2V}. The blue area is excluded by the observation. The 1 and 2σ confidence intervals around the expected median exclusion contour are shown as dark and light-grey areas corresponding to 68 and 95% respectively. The red diamond shows the SM expectation while the fine dashed lines show the theoretical cross section contours. All other Higgs boson couplings are set to the values predicted by the SM.

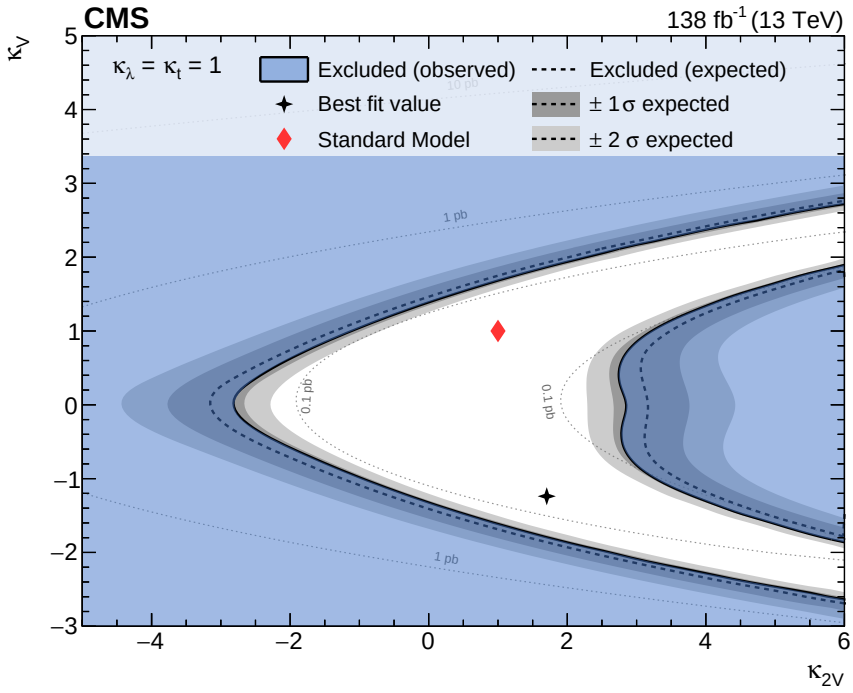

Figure 14: Observed and expected 95% CL exclusion limits on the nonresonant HH production via VBF cross section as a function of the effective couplings κ_V and κ_{2V}. The blue area is excluded by the observation. The 1 and 2σ confidence intervals around the expected median exclusion contour are shown as dark and light-grey areas corresponding to 68 and 95% respectively. The red diamond shows the SM expectation while the fine dashed lines show the theoretical cross section contours. The ggF contribution in this case is set to the SM expectation. All other Higgs boson couplings are set to the values predicted by the SM.

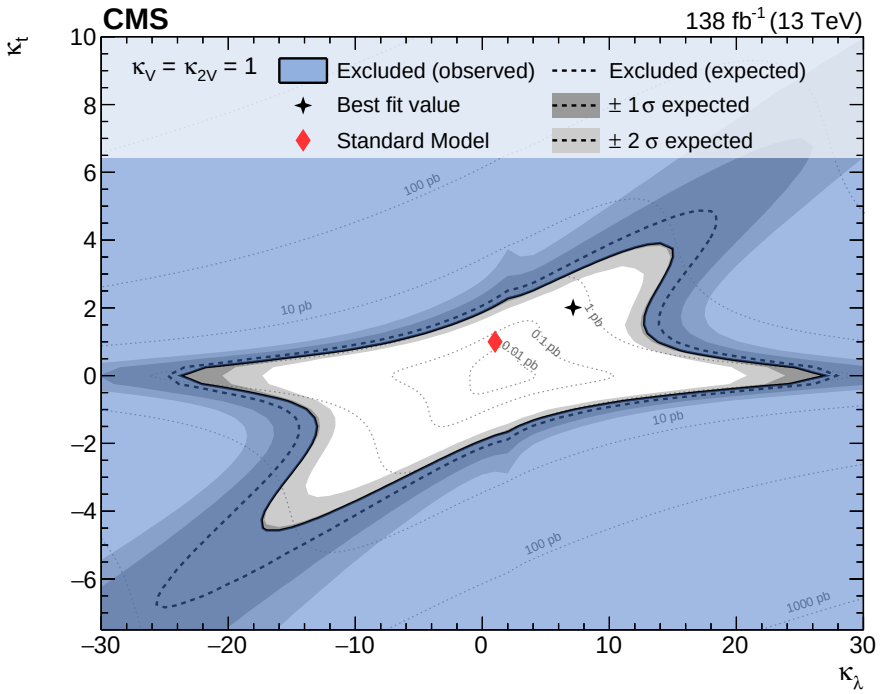

Figure 15: Observed and expected 95% CL exclusion limits on the nonresonant HH production cross section as a function of the effective couplings κ_λ and κ_t. The blue area is excluded by the observation. The 1 and 2σ confidence intervals around the expected median exclusion contour are shown as dark and light-grey areas corresponding to 68 and 95% respectively. The red diamond shows the SM expectation while the fine dashed lines show the theoretical cross section contours. All other Higgs boson couplings are set to the values predicted by the SM.

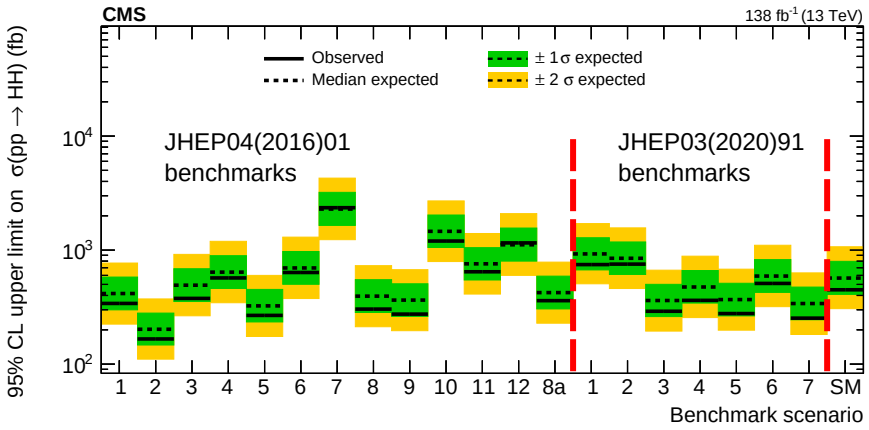

Figure 16: Observed and expected 95% CL upper limits on the nonresonant HH production cross section for two different benchmark scenarios "JHEP04(2016)01" and "JHEP03(2020)91" from Refs. [90, 91]. The green and yellow bands show the 1 and 2σ confidence intervals, corresponding to 68 and 95% CL.

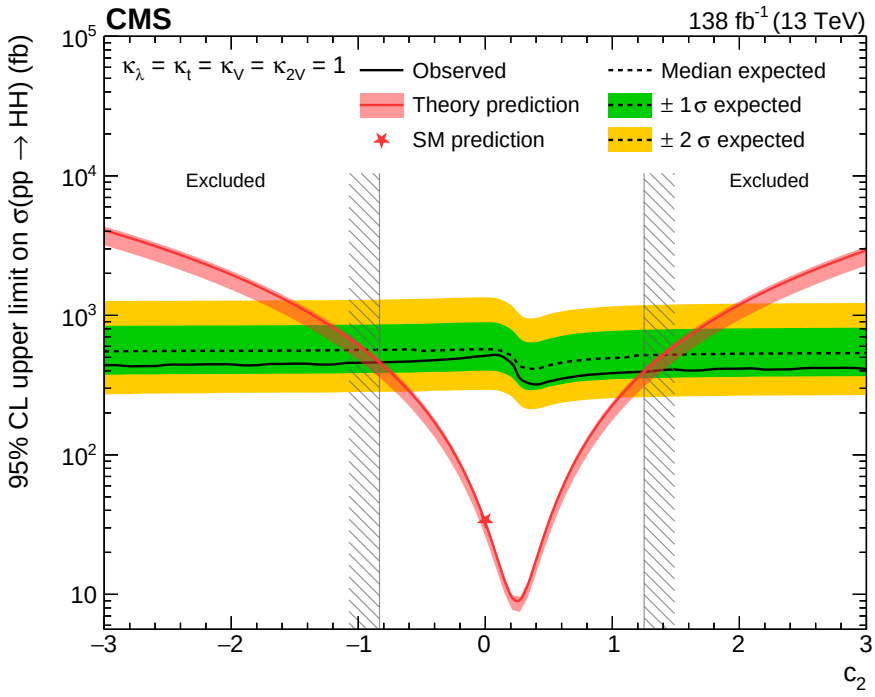

Figure 17: Observed and expected 95% CL upper limits on the nonresonant HH production cross section as a function of the effective coupling c_2. The green and yellow bands show the 1 and 2σ confidence intervals, corresponding to 68 and 95% CL. All other Higgs boson couplings are set to the values predicted in the SM. Overlaid in red (upper) is the curve representing the predicted HH production cross section.

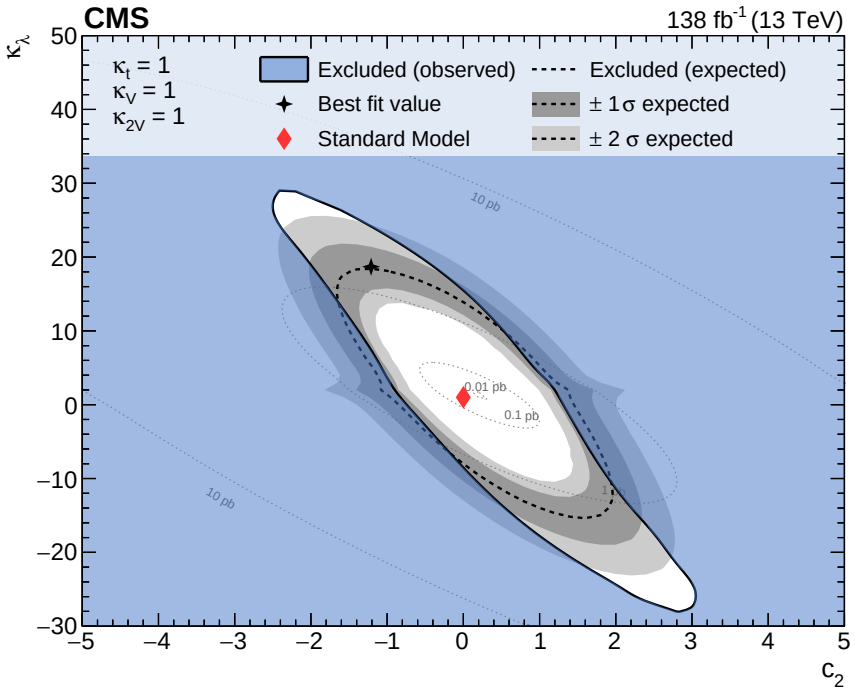

Figure 18: Observed and expected 95% CL exclusion limits on the nonresonant HH production cross section as a function of the effective couplings κ_λ and c_2. The blue area is excluded by the observation. The 1 and 2σ confidence intervals around the expected median exclusion contour are shown as dark and light-grey areas corresponding to 68 and 95% respectively. The red diamond shows the SM expectation while the fine dashed lines show the theoretical cross section contours. All other Higgs boson couplings are set to the values predicted in the SM.

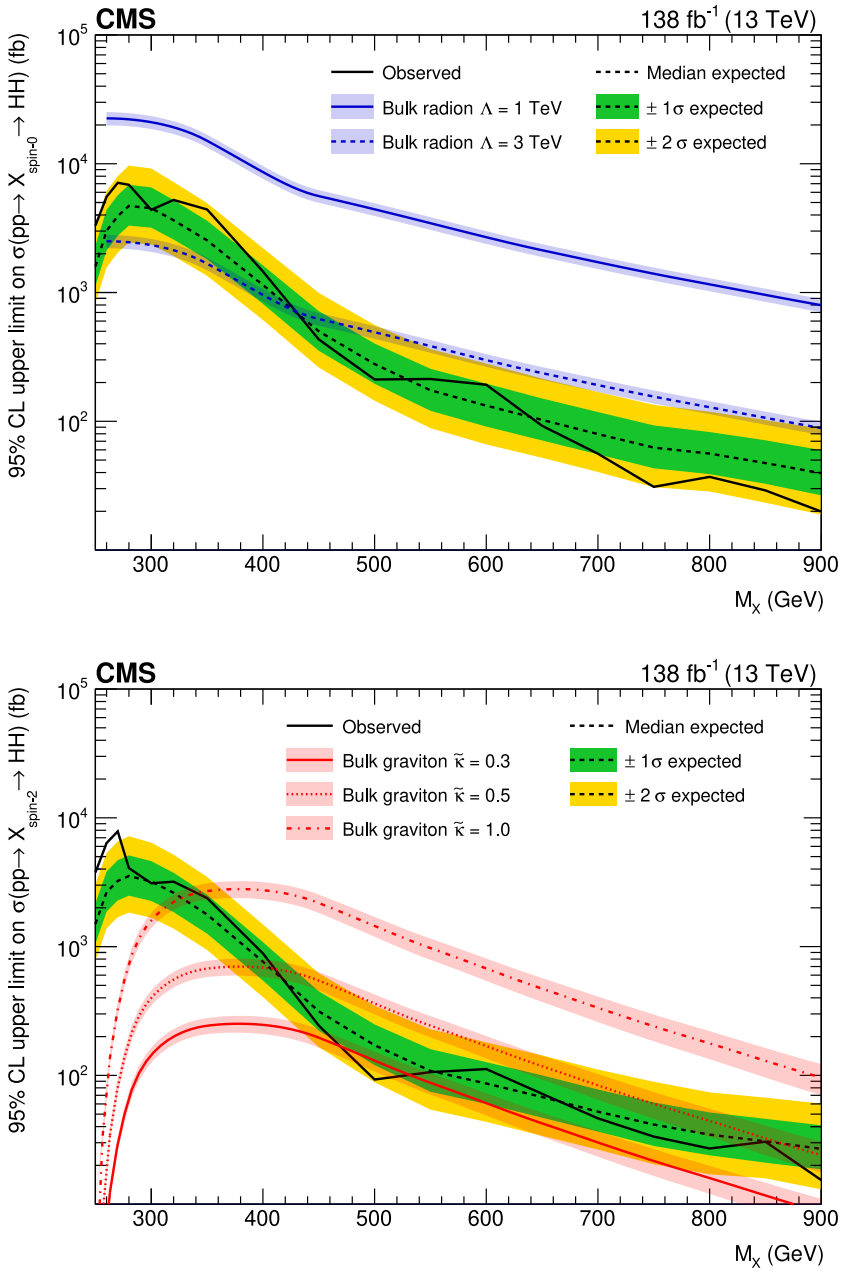

Figure 19: Observed and expected 95% CL upper limits on the production of new particles X of spin-0 (upper) and spin-2 (lower) and mass m_X in the range $250 \leq m_X \leq 900\,\text{GeV}$, which decay to Higgs boson pairs. The green and yellow bands show the 1 and 2σ confidence intervals, corresponding to 68 and 95% CL. Theory predictions in benchmark scenarios for bulk radion (upper) and bulk graviton (lower) models are overlaid.

10 Summary

In this paper, a search for Higgs boson pair production (HH) in the HH $\to b\bar{b}W^+W^-$ decay channel with at least one electron or muon in the final state is presented. The nonresonant and the resonant production mechanisms are studied. No significant deviation from the standard model (SM) background is found. Upper limits are set on the HH production cross section.

The cross section for the inclusive nonresonant HH $\to b\bar{b}W^+W^-$ production is excluded up to a minimum of 14 (expected 18) times the value predicted by the SM at 95% confidence level. Compared to previous results on the same process by the CMS Collaboration, this search represents a significant improvement with a gain in sensitivity by up to a factor of five. The vector boson fusion production is excluded up to 277 (expected 301) times the value predicted by the SM at 95% confidence level.

The limits on the cross sections are also shown as a function of various Higgs boson coupling modifiers and anomalous Higgs boson couplings. The Higgs boson trilinear coupling λ_{HHH} is constrained between $[-7.2, 13.8]$ (expected $[-8.7, 15.2]$) times the value expected in the SM at 95% confidence level. The coupling modifier for the quartic interaction between two Higgs bosons and two W or Z bosons, $\kappa_{2\mathrm{V}}$, is constrained between $[-1.1, 3.2]$ (expected $[-1.4, 3.5]$) at 95% confidence level. The coupling between two top quarks and two Higgs bosons, which is predicted to be zero in the SM, is constrained between $[-0.8,\ 1.3]$ (expected $[-1.0, 1.4]$) at 95% confidence level. The exclusion contours are drawn as a function of the Higgs boson coupling modifiers.

The HH production via a heavy resonance is studied in the mass range from 250 to 900 GeV. Spin-0 and spin-2 scenarios for the resonance are tested and compared to the common theoretical benchmarks of a heavy *CP*-even scalar radion and a graviton. The limits on the resonance production cross section in the spin-0 (2) scenario vary between 5540 (6368) and 20 (15) fb corresponding to the 250 and 900 GeV mass points, respectively. These limits are comparable to those set by the $\gamma\gamma b\bar{b}$ resonant HH search.

Acknowledgments

We congratulate our colleagues in the CERN accelerator departments for the excellent performance of the LHC and thank the technical and administrative staffs at CERN and at other CMS institutes for their contributions to the success of the CMS effort. In addition, we gratefully acknowledge the computing centres and personnel of the Worldwide LHC Computing Grid and other centres for delivering so effectively the computing infrastructure essential to our analyses. Finally, we acknowledge the enduring support for the construction and operation of the LHC, the CMS detector, and the supporting computing infrastructure provided by the following funding agencies: SC (Armenia), BMBWF and FWF (Austria); FNRS and FWO (Belgium); CNPq, CAPES, FAPERJ, FAPERGS, and FAPESP (Brazil); MES and BNSF (Bulgaria); CERN; CAS, MoST, and NSFC (China); MINCIENCIAS (Colombia); MSES and CSF (Croatia); RIF (Cyprus); SENESCYT (Ecuador); ERC PRG, RVTT3 and MoER TK202 (Estonia); Academy of Finland, MEC, and HIP (Finland); CEA and CNRS/IN2P3 (France); SRNSF (Georgia); BMBF, DFG, and HGF (Germany); GSRI (Greece); NKFIH (Hungary); DAE and DST (India); IPM (Iran); SFI (Ireland); INFN (Italy); MSIP and NRF (Republic of Korea); MES (Latvia); LMTLT (Lithuania); MOE and UM (Malaysia); BUAP, CINVESTAV, CONACYT, LNS, SEP, and UASLP-FAI (Mexico); MOS (Montenegro); MBIE (New Zealand); PAEC (Pakistan); MES and NSC (Poland); FCT (Portugal); MESTD (Serbia); MCIN/AEI and PCTI (Spain); MOSTR (Sri Lanka); Swiss Funding Agencies (Switzerland); MST (Taipei); MHESI and NSTDA (Thailand);

TUBITAK and TENMAK (Turkey); NASU (Ukraine); STFC (United Kingdom); DOE and NSF (USA).

Individuals have received support from the Marie-Curie programme and the European Research Council and Horizon 2020 Grant, contract Nos. 675440, 724704, 752730, 758316, 765710, 824093, 101115353,101002207, and COST Action CA16108 (European Union); the Leventis Foundation; the Alfred P. Sloan Foundation; the Alexander von Humboldt Foundation; the Science Committee, project no. 22rl-037 (Armenia); the Belgian Federal Science Policy Office; the Fonds pour la Formation à la Recherche dans l'Industrie et dans l'Agriculture (FRIA-Belgium); the Agentschap voor Innovatie door Wetenschap en Technologie (IWT-Belgium); the F.R.S.-FNRS and FWO (Belgium) under the "Excellence of Science – EOS" – be.h project n. 30820817; the Beijing Municipal Science & Technology Commission, No. Z191100007219010 and Fundamental Research Funds for the Central Universities (China); the Ministry of Education, Youth and Sports (MEYS) of the Czech Republic; the Shota Rustaveli National Science Foundation, grant FR-22-985 (Georgia); the Deutsche Forschungsgemeinschaft (DFG), under Germany's Excellence Strategy – EXC 2121 "Quantum Universe" – 390833306, and under project number 400140256 - GRK2497; the Hellenic Foundation for Research and Innovation (HFRI), Project Number 2288 (Greece); the Hungarian Academy of Sciences, the New National Excellence Program - ÚNKP, the NKFIH research grants K 124845, K 124850, K 128713, K 128786, K 129058, K 131991, K 133046, K 138136, K 143460, K 143477, 2020-2.2.1-ED-2021-00181, and TKP2021-NKTA-64 (Hungary); the Council of Science and Industrial Research, India; ICSC – National Research Centre for High Performance Computing, Big Data and Quantum Computing, funded by the EU NexGeneration program (Italy); the Latvian Council of Science; the Ministry of Education and Science, project no. 2022/WK/14, and the National Science Center, contracts Opus 2021/41/B/ST2/01369 and 2021/43/B/ST2/01552 (Poland); the Fundação para a Ciência e a Tecnologia, grant CEECIND/01334/2018 (Portugal); the National Priorities Research Program by Qatar National Research Fund; MCIN/AEI/10.13039/501100011033, ERDF "a way of making Europe", and the Programa Estatal de Fomento de la Investigación Científica y Técnica de Excelencia María de Maeztu, grant MDM-2017-0765 and Programa Severo Ochoa del Principado de Asturias (Spain); the Chulalongkorn Academic into Its 2nd Century Project Advancement Project, and the National Science, Research and Innovation Fund via the Program Management Unit for Human Resources & Institutional Development, Research and Innovation, grant B37G660013 (Thailand); the Kavli Foundation; the Nvidia Corporation; the SuperMicro Corporation; the Welch Foundation, contract C-1845; and the Weston Havens Foundation (USA).

References

[1] ATLAS Collaboration, "Observation of a new particle in the search for the Standard Model Higgs boson with the ATLAS detector at the LHC", *Phys. Lett. B* **716** (2012) 1, doi:10.1016/j.physletb.2012.08.020, arXiv:1207.7214.

[2] CMS Collaboration, "Observation of a new boson at a mass of 125 GeV with the CMS experiment at the LHC", *Phys. Lett. B* **716** (2012) 30, doi:10.1016/j.physletb.2012.08.021, arXiv:1207.7235.

[3] CMS Collaboration, "Observation of a new boson with mass near 125 GeV in pp collisions at $\sqrt{s} = 7$ and 8 TeV", *JHEP* **06** (2013) 081, doi:10.1007/jhep06(2013)081, arXiv:1303.4571.

[4] ATLAS Collaboration, "A detailed map of Higgs boson interactions by the ATLAS experiment ten years after the discovery", *Nature* **607** (2022) 52, doi:10.1038/s41586-022-04893-w, arXiv:2207.00092.

[5] CMS Collaboration, "A portrait of the Higgs boson by the CMS experiment ten years after the discovery", *Nature* **607** (2022) 60, doi:10.1038/s41586-022-04892-x, arXiv:2207.00043.

[6] CMS Collaboration, "Combined measurements of Higgs boson couplings in proton–proton collisions at $\sqrt{s} = 13\,\text{TeV}$", *Eur. Phys. J. C* **79** (2019) 421, doi:10.1140/epjc/s10052-019-6909-y, arXiv:1809.10733.

[7] ATLAS Collaboration, "Combined measurements of Higgs boson production and decay using up to $80\,\text{fb}^{-1}$ of proton-proton collision data at $\sqrt{s} = 13\,\text{TeV}$ collected with the ATLAS experiment", *Phys. Rev. D* **101** (2020) 012002, doi:10.1103/PhysRevD.101.012002, arXiv:1909.02845.

[8] S. Borowka et al., "Higgs boson pair production in gluon fusion at next-to-leading order with full top-quark mass dependence", *Phys. Rev. Lett.* **117** (2016) 012001, doi:10.1103/PhysRevLett.117.079901, arXiv:1604.06447. [Erratum: Phys.Rev.Lett. 117, 079901 (2016)].

[9] J. Baglio et al., "Gluon fusion into Higgs pairs at NLO QCD and the top mass scheme", *Eur. Phys. J. C* **79** (2019) 459, doi:10.1140/epjc/s10052-019-6973-3, arXiv:1811.05692.

[10] J. Baglio et al., "$gg \to HH$: Combined uncertainties", *Phys. Rev. D* **103** (2021) 056002, doi:10.1103/PhysRevD.103.056002, arXiv:2008.11626.

[11] J. Alison et al., "Higgs boson potential at colliders: Status and perspectives", *Rev. Phys.* **5** (2020) 100045, doi:10.1016/j.revip.2020.100045, arXiv:1910.00012.

[12] M. Grazzini et al., "Higgs boson pair production at NNLO with top quark mass effects", *JHEP* **05** (2018) 059, doi:10.1007/JHEP05(2018)059, arXiv:1803.02463.

[13] F. A. Dreyer and A. Karlberg, "Vector-boson fusion Higgs pair production at N^3LO", *Phys. Rev. D* **98** (2018) 114016, doi:10.1103/PhysRevD.98.114016, arXiv:1811.07906.

[14] LHC Higgs Cross Section Working Group, "Handbook of LHC Higgs cross sections: 3. Higgs properties", *CERN Yellow Rep. Monogr.* **4** (2013) doi:10.5170/CERN-2013-004, arXiv:1307.1347.

[15] K. Cheung, "Phenomenology of radion in Randall-Sundrum scenario", *Phys. Rev. D* **63** (2001) 056007, doi:10.1103/PhysRevD.63.056007, arXiv:hep-ph/0009232.

[16] G. C. Branco et al., "Theory and phenomenology of two-Higgs-doublet models", *Phys. Rep.* **516** (2012) 1, doi:10.1016/j.physrep.2012.02.002, arXiv:1106.0034.

[17] L. Randall and R. Sundrum, "A Large mass hierarchy from a small extra dimension", *Phys. Rev. Lett.* **83** (1999) 3370, doi:10.1103/PhysRevLett.83.3370, arXiv:hep-ph/9905221.

[18] W. D. Goldberger and M. B. Wise, "Modulus stabilization with bulk fields", *Phys. Rev. Lett.* **83** (1999) 4922, doi:10.1103/PhysRevLett.83.4922, arXiv:hep-ph/9907447.

[19] CMS Collaboration, "The CMS experiment at the CERN LHC", *JINST* **3** (2008) S08004, doi:10.1088/1748-0221/3/08/S08004.

[20] CMS Collaboration, "Precision luminosity measurement in proton-proton collisions at $\sqrt{s} = 13\,\text{TeV}$ in 2015 and 2016 at CMS", *Eur. Phys. J. C* **81** (2021) 800, doi:10.1140/epjc/s10052-021-09538-2, arXiv:2104.01927.

[21] CMS Collaboration, "CMS luminosity measurement for the 2017 data-taking period at $\sqrt{s} = 13\,\text{TeV}$", CMS Physics Analysis Summary CMS-PAS-LUM-17-004, 2018.

[22] CMS Collaboration, "CMS luminosity measurement for the 2018 data-taking period at $\sqrt{s} = 13\,\text{TeV}$", CMS Physics Analysis Summary CMS-PAS-LUM-18-002, 2019.

[23] A. L. Read, "Presentation of search results: the CL_s technique", *J. Phys. G* **28** (2002) 2693, doi:10.1088/0954-3899/28/10/313.

[24] T. Junk, "Confidence level computation for combining searches with small statistics", *Nucl. Instrum. Meth. A* **434** (1999) 435, doi:10.1016/S0168-9002(99)00498-2, arXiv:hep-ex/9902006.

[25] ATLAS Collaboration, "Constraints on the Higgs boson self-coupling from single- and double-Higgs production with the ATLAS detector using pp collisions at $\sqrt{s} = 13\,\text{TeV}$", *Phys. Lett. B* **843** (2023) 137745, doi:10.1016/j.physletb.2023.137745, arXiv:2211.01216.

[26] ATLAS Collaboration, "Search for non-resonant Higgs boson pair production in the $2b + 2l + E_\text{T}^\text{miss}$ final state in pp collisions at $\sqrt{s} = 13\,\text{TeV}$ with the ATLAS detector", *JHEP* **02** (2024) 037, doi:10.1007/jhep02(2024)037, arXiv:2310.11286v2.

[27] CMS Collaboration, "Search for resonant and non-resonant Higgs boson pair production in the $\text{b}\bar{\text{b}}\ell\nu\ell\nu$ final state in proton-proton collisions at $\sqrt{s} = 13\,\text{TeV}$", *JHEP* **01** (2018) 054, doi:10.1007/JHEP01(2018)054, arXiv:1708.04188.

[28] E. Bols et al., "Jet flavour classification using DeepJet", *JINST* **15** (2020) P12012, doi:10.1088/1748-0221/15/12/P12012, arXiv:2008.10519.

[29] HEPData record for this analysis, 2024. doi:10.17182/hepdata.149576.

[30] CMS Collaboration, "Performance of the CMS Level-1 trigger in proton-proton collisions at $\sqrt{s} = 13\,\text{TeV}$", *JINST* **15** (2020) P10017, doi:10.1088/1748-0221/15/10/P10017, arXiv:2006.10165.

[31] CMS Collaboration, "The CMS trigger system", *JINST* **12** (2017) P01020, doi:10.1088/1748-0221/12/01/P01020, arXiv:1609.02366.

[32] T. Sjöstrand et al., "An introduction to PYTHIA 8.2", *Comput. Phys. Commun.* **191** (2015) 159, doi:10.1016/j.cpc.2015.01.024, arXiv:1410.3012.

[33] CMS Collaboration, "Event generator tunes obtained from underlying event and multiparton scattering measurements", *Eur. Phys. J. C* **76** (2016) 155, doi:10.1140/epjc/s10052-016-3988-x, arXiv:1512.00815.

[34] CMS Collaboration, "Extraction and validation of a new set of CMS PYTHIA 8 tunes from underlying-event measurements", *Eur. Phys. J. C* **80** (2020) 4, doi:10.1140/epjc/s10052-019-7499-4, arXiv:1903.12179.

[35] NNPDF Collaboration, "Parton distributions with QED corrections", *Nucl. Phys. B* **877** (2013) 290, doi:10.1016/j.nuclphysb.2013.10.010, arXiv:1308.0598.

[36] NNPDF Collaboration, "Parton distributions for the LHC Run II", *JHEP* **04** (2015) 040, doi:10.1007/JHEP04(2015)040, arXiv:1410.8849.

[37] NNPDF Collaboration, "Parton distributions from high-precision collider data", *Eur. Phys. J. C* **77** (2017) 663, doi:10.1140/epjc/s10052-017-5199-5, arXiv:1706.00428.

[38] J. Alwall et al., "The automated computation of tree-level and next-to-leading order differential cross sections, and their matching to parton shower simulations", *JHEP* **07** (2014) 079, doi:10.1007/JHEP07(2014)079, arXiv:1405.0301.

[39] J. Alwall et al., "Comparative study of various algorithms for the merging of parton showers and matrix elements in hadronic collisions", *Eur. Phys. J. C* **53** (2007) 473, doi:10.1140/epjc/s10052-007-0490-5, arXiv:0706.2569.

[40] R. Frederix and S. Frixione, "Merging meets matching in MC@NLO", *JHEP* **12** (2012) 061, doi:10.1007/JHEP12(2012)061, arXiv:1209.6215.

[41] P. Nason, "A new method for combining NLO QCD with shower Monte Carlo algorithms", *JHEP* **11** (2004) 040, doi:10.1088/1126-6708/2004/11/040, arXiv:hep-ph/0409146.

[42] S. Frixione, P. Nason, and C. Oleari, "Matching NLO QCD computations with parton shower simulations: the POWHEG method", *JHEP* **11** (2007) 070, doi:10.1088/1126-6708/2007/11/070, arXiv:0709.2092.

[43] S. Alioli, P. Nason, C. Oleari, and E. Re, "A general framework for implementing NLO calculations in shower Monte Carlo programs: the POWHEG BOX", *JHEP* **06** (2010) 043, doi:10.1007/JHEP06(2010)043, arXiv:1002.2581.

[44] GEANT4 Collaboration, "GEANT4—a simulation toolkit", *Nucl. Instrum. Meth. A* **506** (2003) 250, doi:10.1016/S0168-9002(03)01368-8.

[45] G. Heinrich et al., "Probing the trilinear higgs boson coupling in di-Higgs production at NLO QCD including parton shower effects", *JHEP* **06** (2019) 066, doi:10.1007/jhep06(2019)066, arXiv:1903.08137.

[46] M. Czakon et al., "Top-pair production at the LHC through NNLO QCD and NLO EW", *JHEP* **10** (2017) 186, doi:10.1007/jhep10(2017)186, arXiv:1705.04105v2.

[47] K. Ehatäht and C. Veelken, "Stitching Monte Carlo samples", *Eur. Phys. J. C* **82** (2022) 484, doi:10.1140/epjc/s10052-022-10407-9, arXiv:2106.04360.

[48] K. Melnikov and F. Petriello, "Electroweak gauge boson production at hadron colliders through $O(\alpha_s^2)$", *Phys. Rev. D* **74** (2006) 114017, doi:10.1103/PhysRevD.74.114017, arXiv:hep-ph/0609070.

[49] M. Czakon and A. Mitov, "Top++: A program for the calculation of the top-pair cross section at hadron colliders", *Comput. Phys. Commun.* **185** (2014) 2930, doi:10.1016/j.cpc.2014.06.021, arXiv:1112.5675.

[50] CMS Collaboration, "Measurement of differential cross sections for Z boson production in association with jets in proton-proton collisions at $\sqrt{s} = 13$ TeV", *Eur. Phys. J. C* **78** (2018) 965, doi:10.1140/epjc/s10052-018-6373-0, arXiv:1804.05252.

[51] CMS Collaboration, "Particle-flow reconstruction and global event description with the CMS detector", *JINST* **12** (2017) P10003, doi:10.1088/1748-0221/12/10/P10003, arXiv:1706.04965.

[52] CMS Collaboration, "Technical proposal for the Phase-II upgrade of the Compact Muon Solenoid", CMS Technical Proposal CERN-LHCC-2015-010, CMS-TDR-15-02, 2015.

[53] M. Cacciari, G. P. Salam, and G. Soyez, "The anti-k_{T} jet clustering algorithm", *JHEP* **04** (2008) 063, doi:10.1088/1126-6708/2008/04/063, arXiv:0802.1189.

[54] M. Cacciari, G. P. Salam, and G. Soyez, "FastJet user manual", *Eur. Phys. J. C* **72** (2012) 1896, doi:10.1140/epjc/s10052-012-1896-2, arXiv:1111.6097.

[55] CMS Collaboration, "Jet energy scale and resolution measurement with Run 2 legacy data collected by CMS at 13 TeV", CMS Detector Performance Note CERN-CMS-DP-2021-033, 2021.

[56] CMS Collaboration, "Jet energy scale and resolution in the CMS experiment in pp collisions at 8 TeV", *JINST* **12** (2017) P02014, doi:10.1088/1748-0221/12/02/P02014, arXiv:1607.03663.

[57] CMS Collaboration, "Pileup mitigation at CMS in 13 TeV data", *JINST* **15** (2020) P09018, doi:10.1088/1748-0221/15/09/P09018, arXiv:2003.00503.

[58] CMS Collaboration, "Performance of the DeepJet b tagging algorithm using 41.9 fb^{-1} of data from proton-proton collisions at 13 TeV with Phase 1 CMS detector", CMS Detector Performance Note CMS-DP-2018-058, 2018.

[59] CMS Collaboration, "A Deep Neural Network for Simultaneous Estimation of b Jet Energy and Resolution", *Comput. Softw. Big Sci.* **4** (2020) 10, doi:10.1007/s41781-020-00041-z, arXiv:1912.06046.

[60] D. Bertolini, P. Harris, M. Low, and N. Tran, "Pileup per particle identification", *JHEP* **10** (2014) 059, doi:10.1007/JHEP10(2014)059, arXiv:1407.6013.

[61] CMS Collaboration, "Identification of heavy-flavour jets with the CMS detector in pp collisions at 13 TeV", *JINST* **13** (2018) P05011, doi:10.1088/1748-0221/13/05/P05011, arXiv:1712.07158.

[62] M. Dasgupta, A. Fregoso, S. Marzani, and G. P. Salam, "Towards an understanding of jet substructure", *JHEP* **09** (2013) 029, doi:10.1007/JHEP09(2013)029, arXiv:1307.0007.

[63] J. M. Butterworth, A. R. Davison, M. Rubin, and G. P. Salam, "Jet substructure as a new Higgs search channel at the LHC", *Phys. Rev. Lett.* **100** (2008) 242001, doi:10.1103/PhysRevLett.100.242001, arXiv:0802.2470.

[64] J. Thaler and K. Van Tilburg, "Identifying boosted objects with N-subjettiness", *JHEP* **03** (2011) 015, doi:10.1007/JHEP03(2011)015, arXiv:1011.2268.

[65] CMS Collaboration, "Performance of electron reconstruction and selection with the CMS detector in proton-proton collisions at $\sqrt{s} = 8$ TeV", *JINST* **10** (2015) P06005, doi:10.1088/1748-0221/10/06/P06005, arXiv:1502.02701.

[66] CMS Collaboration, "Electron and photon reconstruction and identification with the CMS experiment at the CERN LHC", *JINST* **16** (2021) P05014, doi:10.1088/1748-0221/16/05/P05014, arXiv:2012.06888.

[67] A. Hoecker et al., "TMVA — toolkit for multivariate data analysis", *PoS* **ACAT** (2007) 040, doi:10.48550/arXiv.physics/0703039, arXiv:physics/0703039.

[68] CMS Collaboration, "Performance of CMS muon reconstruction in pp collision events at $\sqrt{s} = 7$ TeV", *JINST* **7** (2012) P10002, doi:10.1088/1748-0221/7/10/P10002, arXiv:1206.4071.

[69] CMS Collaboration, "Performance of the CMS muon detector and muon reconstruction with proton-proton collisions at $\sqrt{s} = 13$ TeV", *JINST* **13** (2018) P06015, doi:10.1088/1748-0221/13/06/P06015, arXiv:1804.04528.

[70] M. Cacciari, G. P. Salam, and G. Soyez, "The catchment area of jets", *JHEP* **04** (2008) 005, doi:10.1088/1126-6708/2008/04/005, arXiv:0802.1188.

[71] M. Cacciari and G. P. Salam, "Pileup subtraction using jet areas", *Phys. Lett. B* **659** (2008) 119, doi:10.1016/j.physletb.2007.09.077, arXiv:0707.1378.

[72] CMS Collaboration, "Measurement of the Higgs boson production rate in association with top quarks in final states with electrons, muons, and hadronically decaying tau leptons at $\sqrt{s} = 13$ TeV", *Eur. Phys. J. C* **81** (2021) 378, doi:10.1140/epjc/s10052-021-09014-x, arXiv:2011.03652.

[73] CMS Collaboration, "Performance of missing transverse momentum reconstruction in proton-proton collisions at $\sqrt{s} = 13$ TeV using the CMS detector", *JINST* **14** (2019) P07004, doi:10.1088/1748-0221/14/07/P07004, arXiv:1903.06078.

[74] P. D. Group, "Review of Particle Physics", *PTEP* **2022** (2022) 083C01, doi:10.1093/ptep/ptac097.

[75] CMS Collaboration, "Identification of hadronic tau lepton decays using a deep neural network", *JINST* **17** (2022) P07023, doi:10.1088/1748-0221/17/07/P07023, arXiv:2201.08458.

[76] CMS Collaboration, "Search for nonresonant Higgs boson pair production in final state with two bottom quarks and two tau leptons in proton-proton collisions at $\sqrt{s} = 13$ TeV", *Phys. Lett. B* **842** (2023) 137531, doi:10.1016/j.physletb.2022.137531, arXiv:2206.09401.

[77] ATLAS and CMS Collaborations, and LHC Higgs Combination Group, "Procedure for the LHC Higgs boson search combination in Summer 2011", Technical Report CMS-NOTE-2011-005, ATL-PHYS-PUB-2011-11, 2011.

[78] P. Baldi et al., "Parameterized neural networks for high-energy physics", *Eur. Phys. J. C* **76** (2016) 235, doi:10.1140/epjc/s10052-016-4099-4, arXiv:1601.07913.

[79] M. Erdmann, E. Geiser, Y. Rath, and M. Rieger, "Lorentz Boost Networks: Autonomous physics-inspired feature engineering", *JINST* **14** (2019) P06006, doi:10.1088/1748-0221/14/06/p06006, arXiv:1812.09722.

[80] T. Huang et al., "Resonant di-Higgs boson production in the $b\bar{b}WW$ channel: Probing the electroweak phase transition at the LHC", *Phys. Rev. D* **96** (2017) 035007, doi:10.1103/PhysRevD.96.035007, arXiv:1701.04442.

[81] CMS Collaboration, "Evidence for associated production of a Higgs boson with a top quark pair in final states with electrons, muons, and hadronically decaying τ leptons at $\sqrt{s} = 13\,\text{TeV}$", *JHEP* **08** (2018) 066, doi:10.1007/jhep08(2018)066, arXiv:1803.05485.

[82] L.-S. Ling et al., "NNLO QCD corrections to Higgs pair production via vector boson fusion at hadron colliders", *Phys. Rev. D* **89** (2014) 073001, doi:10.1103/PhysRevD.89.073001, arXiv:1401.7754.

[83] F. A. Dreyer and A. Karlberg, "Fully differential vector-boson fusion Higgs pair production at next-to-next-to-leading order", *Phys. Rev. D* **99** (2019) 074028, doi:10.1103/PhysRevD.99.074028, arXiv:1811.07918.

[84] B. Cabouat and T. Sjöstrand, "Some dipole shower studies", *Eur. Phys. J. C* **78** (2018) 226, doi:10.1140/epjc/s10052-018-5645-z, arXiv:1710.00391v2.

[85] D. de Florian, I. Fabre, and J. Mazzitelli, "Higgs boson pair production at NNLO in QCD including dimension 6 operators", *JHEP* **10** (2017) 215, doi:10.1007/JHEP10(2017)215, arXiv:1704.05700.

[86] LHC Higgs Cross Section Working Group, "Handbook of LHC Higgs Cross Sections: 4. Deciphering the nature of the Higgs sector", *CERN Yellow Rep. Monogr.* **2** (2017) doi:10.23731/CYRM-2017-002, arXiv:1610.07922.

[87] CMS Collaboration, "Measurement of the inelastic proton-proton cross section at $\sqrt{s} = 13\,\text{TeV}$", *JHEP* **07** (2018) 161, doi:10.1007/JHEP07(2018)161, arXiv:1802.02613.

[88] G. Cowan, K. Cranmer, E. Gross, and O. Vitells, "Asymptotic formulae for likelihood-based tests of new physics", *Eur. Phys. J. C* **71** (2011) 1554, doi:10.1140/epjc/s10052-011-1554-0, arXiv:1007.1727. [Erratum: Eur.Phys.J.C 73, 2501 (2013)].

[89] CMS Collaboration, "Search for nonresonant Higgs boson pair production in final states with two bottom quarks and two photons in proton-proton collisions at $\sqrt{s} = 13\,\text{TeV}$", *JHEP* **03** (2021) 257, doi:10.1007/jhep03(2021)257, arXiv:2011.12373.

[90] A. Carvalho et al., "Higgs pair production: choosing benchmarks with cluster analysis", *JHEP* **04** (2016) 1, doi:10.1007/jhep04(2016)126, arXiv:1507.02245.

[91] M. Capozi and G. Heinrich, "Exploring anomalous couplings in Higgs boson pair production through shape analysis", *JHEP* **03** (2020) 091, doi:10.1007/JHEP03(2020)091, arXiv:1908.08923.

[92] CMS Collaboration, "Search for heavy resonances decaying to a pair of Lorentz-boosted Higgs bosons in final states with leptons and a bottom quark pair at $\sqrt{s}$ = 13 TeV", *JHEP* **05** (2022) 005, doi:10.1007/jhep05(2022)005, arXiv:2112.03161v2.

[93] CMS Collaboration, "Search for a new resonance decaying into two spin-0 bosons in a final state with two photons and two bottom quarks in proton-proton collisions at $\sqrt{s} = 13$ TeV", 10, 2023. arXiv:2310.01643. Submitted to *JHEP*.

[94] A. Carvalho, "Gravity particles from warped extra dimensions, predictions for LHC", 2014. arXiv:1404.0102.

[95] M. Gouzevitch et al., "Scale-invariant resonance tagging in multijet events and new physics in Higgs pair production", *JHEP* **07** (2013) 148, doi:10.1007/JHEP07(2013)148, arXiv:1303.6636.

A The CMS Collaboration

Yerevan Physics Institute, Yerevan, Armenia
A. Hayrapetyan, A. Tumasyan[1]

Institut für Hochenergiephysik, Vienna, Austria
W. Adam, J.W. Andrejkovic, T. Bergauer, S. Chatterjee, K. Damanakis, M. Dragicevic, A. Escalante Del Valle, P.S. Hussain, M. Jeitler[2], N. Krammer, D. Liko, I. Mikulec, J. Schieck[2], R. Schöfbeck, D. Schwarz, M. Sonawane, S. Templ, W. Waltenberger, C.-E. Wulz[2]

Universiteit Antwerpen, Antwerpen, Belgium
M.R. Darwish[3], T. Janssen, P. Van Mechelen

Vrije Universiteit Brussel, Brussel, Belgium
E.S. Bols, J. D'Hondt, S. Dansana, A. De Moor, M. Delcourt, H. El Faham, S. Lowette, I. Makarenko, D. Müller, A.R. Sahasransu, S. Tavernier, M. Tytgat[4], S. Van Putte, D. Vannerom

Université Libre de Bruxelles, Bruxelles, Belgium
B. Clerbaux, G. De Lentdecker, L. Favart, D. Hohov, J. Jaramillo, A. Khalilzadeh, K. Lee, M. Mahdavikhorrami, A. Malara, S. Paredes, L. Pétré, N. Postiau, L. Thomas, M. Vanden Bemden, C. Vander Velde, P. Vanlaer

Ghent University, Ghent, Belgium
M. De Coen, D. Dobur, Y. Hong, J. Knolle, L. Lambrecht, G. Mestdach, C. Rendón, A. Samalan, K. Skovpen, N. Van Den Bossche, L. Wezenbeek

Université Catholique de Louvain, Louvain-la-Neuve, Belgium
A. Benecke, G. Bruno, C. Caputo, C. Delaere, I.S. Donertas, A. Giammanco, K. Jaffel, Sa. Jain, V. Lemaitre, J. Lidrych, P. Mastrapasqua, K. Mondal, T.T. Tran, S. Wertz

Centro Brasileiro de Pesquisas Fisicas, Rio de Janeiro, Brazil
G.A. Alves, E. Coelho, C. Hensel, T. Menezes De Oliveira, A. Moraes, P. Rebello Teles, M. Soeiro

Universidade do Estado do Rio de Janeiro, Rio de Janeiro, Brazil
W.L. Aldá Júnior, M. Alves Gallo Pereira, M. Barroso Ferreira Filho, H. Brandao Malbouisson, W. Carvalho, J. Chinellato[5], E.M. Da Costa, G.G. Da Silveira[6], D. De Jesus Damiao, S. Fonseca De Souza, J. Martins[7], C. Mora Herrera, K. Mota Amarilo, L. Mundim, H. Nogima, A. Santoro, S.M. Silva Do Amaral, A. Sznajder, M. Thiel, A. Vilela Pereira

Universidade Estadual Paulista, Universidade Federal do ABC, São Paulo, Brazil
C.A. Bernardes[6], L. Calligaris, T.R. Fernandez Perez Tomei, E.M. Gregores, P.G. Mercadante, S.F. Novaes, B. Orzari, Sandra S. Padula

Institute for Nuclear Research and Nuclear Energy, Bulgarian Academy of Sciences, Sofia, Bulgaria
A. Aleksandrov, G. Antchev, R. Hadjiiska, P. Iaydjiev, M. Misheva, M. Shopova, G. Sultanov

University of Sofia, Sofia, Bulgaria
A. Dimitrov, T. Ivanov, L. Litov, B. Pavlov, P. Petkov, A. Petrov, E. Shumka

Instituto De Alta Investigación, Universidad de Tarapacá, Casilla 7 D, Arica, Chile
S. Keshri, S. Thakur

Beihang University, Beijing, China
T. Cheng, Q. Guo, T. Javaid, M. Mittal, L. Yuan

Department of Physics, Tsinghua University, Beijing, China
G. Bauer[8,9], Z. Hu, J. Liu, K. Yi[8,10]

Institute of High Energy Physics, Beijing, China
G.M. Chen[11], H.S. Chen[11], M. Chen[11], F. Iemmi, C.H. Jiang, A. Kapoor[12], H. Liao, Z.-A. Liu[13], F. Monti, M.A. Shahzad[11], R. Sharma[14], J.N. Song[13], J. Tao, C. Wang[11], J. Wang, Z. Wang[11], H. Zhang

State Key Laboratory of Nuclear Physics and Technology, Peking University, Beijing, China
A. Agapitos, Y. Ban, A. Levin, C. Li, Q. Li, Y. Mao, S.J. Qian, X. Sun, D. Wang, H. Yang, C. Zhou

Sun Yat-Sen University, Guangzhou, China
Z. You

University of Science and Technology of China, Hefei, China
N. Lu

Institute of Modern Physics and Key Laboratory of Nuclear Physics and Ion-beam Application (MOE) - Fudan University, Shanghai, China
X. Gao[15], D. Leggat, H. Okawa, Y. Zhang

Zhejiang University, Hangzhou, Zhejiang, China
Z. Lin, C. Lu, M. Xiao

Universidad de Los Andes, Bogota, Colombia
C. Avila, D.A. Barbosa Trujillo, A. Cabrera, C. Florez, J. Fraga, J.A. Reyes Vega

Universidad de Antioquia, Medellin, Colombia
J. Mejia Guisao, F. Ramirez, M. Rodriguez, J.D. Ruiz Alvarez

University of Split, Faculty of Electrical Engineering, Mechanical Engineering and Naval Architecture, Split, Croatia
D. Giljanovic, N. Godinovic, D. Lelas, A. Sculac

University of Split, Faculty of Science, Split, Croatia
M. Kovac, T. Sculac

Institute Rudjer Boskovic, Zagreb, Croatia
P. Bargassa, V. Brigljevic, B.K. Chitroda, D. Ferencek, S. Mishra, A. Starodumov[16], T. Susa

University of Cyprus, Nicosia, Cyprus
A. Attikis, K. Christoforou, S. Konstantinou, J. Mousa, C. Nicolaou, F. Ptochos, P.A. Razis, H. Rykaczewski, H. Saka, A. Stepennov

Charles University, Prague, Czech Republic
M. Finger, M. Finger Jr., A. Kveton

Escuela Politecnica Nacional, Quito, Ecuador
E. Ayala

Universidad San Francisco de Quito, Quito, Ecuador
E. Carrera Jarrin

Academy of Scientific Research and Technology of the Arab Republic of Egypt, Egyptian Network of High Energy Physics, Cairo, Egypt
S. Elgammal[17], A. Ellithi Kamel[18]

Center for High Energy Physics (CHEP-FU), Fayoum University, El-Fayoum, Egypt
A. Lotfy, M.A. Mahmoud

National Institute of Chemical Physics and Biophysics, Tallinn, Estonia
R.K. Dewanjee[19], K. Ehataht, M. Kadastik, T. Lange, S. Nandan, C. Nielsen, J. Pata, M. Raidal, L. Tani, C. Veelken

Department of Physics, University of Helsinki, Helsinki, Finland
H. Kirschenmann, K. Osterberg, M. Voutilainen

Helsinki Institute of Physics, Helsinki, Finland
S. Bharthuar, E. Brücken, F. Garcia, J. Havukainen, K.T.S. Kallonen, M.S. Kim, R. Kinnunen, T. Lampén, K. Lassila-Perini, S. Lehti, T. Lindén, M. Lotti, L. Martikainen, M. Myllymäki, M.m. Rantanen, H. Siikonen, E. Tuominen, J. Tuominiemi

Lappeenranta-Lahti University of Technology, Lappeenranta, Finland
P. Luukka, H. Petrow, T. Tuuva[†]

IRFU, CEA, Université Paris-Saclay, Gif-sur-Yvette, France
M. Besancon, F. Couderc, M. Dejardin, D. Denegri, J.L. Faure, F. Ferri, S. Ganjour, P. Gras, G. Hamel de Monchenault, V. Lohezic, J. Malcles, J. Rander, A. Rosowsky, M.Ö. Sahin, A. Savoy-Navarro[20], P. Simkina, M. Titov

Laboratoire Leprince-Ringuet, CNRS/IN2P3, Ecole Polytechnique, Institut Polytechnique de Paris, Palaiseau, France
C. Baldenegro Barrera, F. Beaudette, A. Buchot Perraguin, P. Busson, A. Cappati, C. Charlot, F. Damas, O. Davignon, A. De Wit, G. Falmagne, B.A. Fontana Santos Alves, S. Ghosh, A. Gilbert, R. Granier de Cassagnac, A. Hakimi, B. Harikrishnan, L. Kalipoliti, G. Liu, J. Motta, M. Nguyen, C. Ochando, L. Portales, R. Salerno, U. Sarkar, J.B. Sauvan, Y. Sirois, A. Tarabini, E. Vernazza, A. Zabi, A. Zghiche

Université de Strasbourg, CNRS, IPHC UMR 7178, Strasbourg, France
J.-L. Agram[21], J. Andrea, D. Apparu, D. Bloch, J.-M. Brom, E.C. Chabert, C. Collard, S. Falke, U. Goerlach, C. Grimault, R. Haeberle, A.-C. Le Bihan, M.A. Sessini, P. Van Hove

Institut de Physique des 2 Infinis de Lyon (IP2I), Villeurbanne, France
S. Beauceron, B. Blancon, G. Boudoul, N. Chanon, J. Choi, D. Contardo, P. Depasse, C. Dozen[22], H. El Mamouni, J. Fay, S. Gascon, M. Gouzevitch, C. Greenberg, G. Grenier, B. Ille, I.B. Laktineh, M. Lethuillier, L. Mirabito, S. Perries, A. Purohit, M. Vander Donckt, P. Verdier, J. Xiao

Georgian Technical University, Tbilisi, Georgia
A. Khvedelidze[16], I. Lomidze, Z. Tsamalaidze[16]

RWTH Aachen University, I. Physikalisches Institut, Aachen, Germany

V. Botta, L. Feld, K. Klein, M. Lipinski, D. Meuser, A. Pauls, N. Röwert, M. Teroerde

RWTH Aachen University, III. Physikalisches Institut A, Aachen, Germany
S. Diekmann, A. Dodonova, N. Eich, D. Eliseev, F. Engelke, M. Erdmann, P. Fackeldey, B. Fischer, T. Hebbeker, K. Hoepfner, F. Ivone, A. Jung, M.y. Lee, L. Mastrolorenzo, M. Merschmeyer, A. Meyer, S. Mukherjee, D. Noll, A. Novak, F. Nowotny, A. Pozdnyakov, Y. Rath, W. Redjeb, F. Rehm, H. Reithler, V. Sarkisovi, A. Schmidt, S.C. Schuler, A. Sharma, A. Stein, F. Torres Da Silva De Araujo[23], L. Vigilante, S. Wiedenbeck, S. Zaleski

RWTH Aachen University, III. Physikalisches Institut B, Aachen, Germany
C. Dziwok, G. Flügge, W. Haj Ahmad[24], T. Kress, A. Nowack, O. Pooth, A. Stahl, T. Ziemons, A. Zotz

Deutsches Elektronen-Synchrotron, Hamburg, Germany
H. Aarup Petersen, M. Aldaya Martin, J. Alimena, S. Amoroso, Y. An, S. Baxter, M. Bayatmakou, H. Becerril Gonzalez, O. Behnke, A. Belvedere, S. Bhattacharya, F. Blekman[25], K. Borras[26], D. Brunner, A. Campbell, A. Cardini, C. Cheng, F. Colombina, S. Consuegra Rodríguez, G. Correia Silva, M. De Silva, G. Eckerlin, D. Eckstein, L.I. Estevez Banos, O. Filatov, E. Gallo[25], A. Geiser, A. Giraldi, G. Greau, V. Guglielmi, M. Guthoff, A. Hinzmann, A. Jafari[27], L. Jeppe, N.Z. Jomhari, B. Kaech, M. Kasemann, H. Kaveh, C. Kleinwort, R. Kogler, M. Komm, D. Krücker, W. Lange, D. Leyva Pernia, K. Lipka[28], W. Lohmann[29], R. Mankel, I.-A. Melzer-Pellmann, M. Mendizabal Morentin, J. Metwally, A.B. Meyer, G. Milella, A. Mussgiller, A. Nürnberg, Y. Otarid, D. Pérez Adán, E. Ranken, A. Raspereza, B. Ribeiro Lopes, J. Rübenach, A. Saggio, M. Scham[30,26], S. Schnake[26], P. Schütze, C. Schwanenberger[25], D. Selivanova, M. Shchedrolosiev, R.E. Sosa Ricardo, L.P. Sreelatha Pramod, D. Stafford, F. Vazzoler, A. Ventura Barroso, R. Walsh, Q. Wang, Y. Wen, K. Wichmann, L. Wiens[26], C. Wissing, S. Wuchterl, Y. Yang, A. Zimermmane Castro Santos

University of Hamburg, Hamburg, Germany
A. Albrecht, S. Albrecht, M. Antonello, S. Bein, L. Benato, M. Bonanomi, P. Connor, M. Eich, K. El Morabit, Y. Fischer, A. Fröhlich, C. Garbers, E. Garutti, A. Grohsjean, M. Hajheidari, J. Haller, H.R. Jabusch, G. Kasieczka, P. Keicher, R. Klanner, W. Korcari, T. Kramer, V. Kutzner, F. Labe, J. Lange, A. Lobanov, C. Matthies, A. Mehta, L. Moureaux, M. Mrowietz, A. Nigamova, Y. Nissan, A. Paasch, K.J. Pena Rodriguez, T. Quadfasel, B. Raciti, M. Rieger, D. Savoiu, J. Schindler, P. Schleper, M. Schröder, J. Schwandt, M. Sommerhalder, H. Stadie, G. Steinbrück, A. Tews, M. Wolf

Karlsruher Institut fuer Technologie, Karlsruhe, Germany
S. Brommer, M. Burkart, E. Butz, T. Chwalek, A. Dierlamm, A. Droll, N. Faltermann, M. Giffels, A. Gottmann, F. Hartmann[31], R. Hofsaess, M. Horzela, U. Husemann, M. Klute, R. Koppenhöfer, M. Link, A. Lintuluoto, S. Maier, S. Mitra, M. Mormile, Th. Müller, M. Neukum, M. Oh, G. Quast, K. Rabbertz, B. Regnery, N. Shadskiy, I. Shvetsov, H.J. Simonis, N. Trevisani, R. Ulrich, J. van der Linden, R.F. Von Cube, M. Wassmer, S. Wieland, F. Wittig, R. Wolf, S. Wunsch, X. Zuo

Institute of Nuclear and Particle Physics (INPP), NCSR Demokritos, Aghia Paraskevi,

Greece
G. Anagnostou, P. Assiouras, G. Daskalakis, A. Kyriakis, A. Papadopoulos[31], A. Stakia

National and Kapodistrian University of Athens, Athens, Greece
P. Kontaxakis, G. Melachroinos, A. Panagiotou, I. Papavergou, I. Paraskevas, N. Saoulidou, K. Theofilatos, E. Tziaferi, K. Vellidis, I. Zisopoulos

National Technical University of Athens, Athens, Greece
G. Bakas, T. Chatzistavrou, G. Karapostoli, K. Kousouris, I. Papakrivopoulos, E. Siamarkou, G. Tsipolitis, A. Zacharopoulou

University of Ioánnina, Ioánnina, Greece
K. Adamidis, I. Bestintzanos, I. Evangelou, C. Foudas, P. Gianneios, C. Kamtsikis, P. Katsoulis, P. Kokkas, P.G. Kosmoglou Kioseoglou, N. Manthos, I. Papadopoulos, J. Strologas

HUN-REN Wigner Research Centre for Physics, Budapest, Hungary
M. Bartók[32], C. Hajdu, D. Horvath[33,34], F. Sikler, V. Veszpremi

MTA-ELTE Lendület CMS Particle and Nuclear Physics Group, Eötvös Loránd University, Budapest, Hungary
M. Csanád, K. Farkas, M.M.A. Gadallah[35], Á. Kadlecsik, P. Major, K. Mandal, G. Pásztor, A.J. Rádl[36], G.I. Veres

Faculty of Informatics, University of Debrecen, Debrecen, Hungary
P. Raics, B. Ujvari[37], G. Zilizi

Institute of Nuclear Research ATOMKI, Debrecen, Hungary
G. Bencze, S. Czellar, J. Karancsi[32], J. Molnar, Z. Szillasi

Karoly Robert Campus, MATE Institute of Technology, Gyongyos, Hungary
T. Csorgo[36], F. Nemes[36], T. Novak

Panjab University, Chandigarh, India
J. Babbar, S. Bansal, S.B. Beri, V. Bhatnagar, G. Chaudhary, S. Chauhan, N. Dhingra[38], R. Gupta, A. Kaur, A. Kaur, H. Kaur, M. Kaur, S. Kumar, M. Meena, K. Sandeep, T. Sheokand, J.B. Singh, A. Singla

University of Delhi, Delhi, India
A. Ahmed, A. Bhardwaj, A. Chhetri, B.C. Choudhary, A. Kumar, M. Naimuddin, K. Ranjan, S. Saumya

Saha Institute of Nuclear Physics, HBNI, Kolkata, India
S. Acharya[39], S. Baradia, S. Barman[40], S. Bhattacharya, D. Bhowmik, S. Dutta, S. Dutta, B. Gomber[39], P. Palit, G. Saha, B. Sahu[39], S. Sarkar

Indian Institute of Technology Madras, Madras, India
M.M. Ameen, P.K. Behera, S.C. Behera, S. Chatterjee, P. Jana, P. Kalbhor, J.R. Komaragiri[41], D. Kumar[41], L. Panwar[41], R. Pradhan, P.R. Pujahari, N.R. Saha, A. Sharma, A.K. Sikdar, S. Verma

Tata Institute of Fundamental Research-A, Mumbai, India
T. Aziz, I. Das, S. Dugad, M. Kumar, G.B. Mohanty, P. Suryadevara

Tata Institute of Fundamental Research-B, Mumbai, India
A. Bala, S. Banerjee, R.M. Chatterjee, M. Guchait, Sh. Jain, S. Karmakar,

S. Kumar, G. Majumder, K. Mazumdar, S. Mukherjee, S. Parolia, A. Thachayath

National Institute of Science Education and Research, An OCC of Homi Bhabha National Institute, Bhubaneswar, Odisha, India
S. Bahinipati[42], A.K. Das, C. Kar, D. Maity[43], P. Mal, T. Mishra, V.K. Muraleedharan Nair Bindhu[43], K. Naskar[43], A. Nayak[43], P. Sadangi, P. Saha, S.K. Swain, S. Varghese[43], D. Vats[43]

Indian Institute of Science Education and Research (IISER), Pune, India
A. Alpana, S. Dube, B. Kansal, A. Laha, A. Rastogi, S. Sharma

Isfahan University of Technology, Isfahan, Iran
H. Bakhshiansohi[44], E. Khazaie[44], M. Zeinali[45]

Institute for Research in Fundamental Sciences (IPM), Tehran, Iran
S. Chenarani[46], S.M. Etesami, M. Khakzad, M. Mohammadi Najafabadi

University College Dublin, Dublin, Ireland
M. Grunewald

INFN Sezione di Bari[a], Università di Bari[b], Politecnico di Bari[c], Bari, Italy
M. Abbrescia[a,b], R. Aly[a,c,47], A. Colaleo[a,b], D. Creanza[a,c], B. D'Anzi[a,b], N. De Filippis[a,c], M. De Palma[a,b], A. Di Florio[a,c], W. Elmetenawee[a,b,47], L. Fiore[a], G. Iaselli[a,c], G. Maggi[a,c], M. Maggi[a], I. Margjeka[a,b], V. Mastrapasqua[a,b], S. My[a,b], S. Nuzzo[a,b], A. Pellecchia[a,b], A. Pompili[a,b], G. Pugliese[a,c], R. Radogna[a], G. Ramirez-Sanchez[a,c], D. Ramos[a], A. Ranieri[a], L. Silvestris[a], F.M. Simone[a,b], Ü. Sözbilir[a], A. Stamerra[a], R. Venditti[a], P. Verwilligen[a], A. Zaza[a,b]

INFN Sezione di Bologna[a], Università di Bologna[b], Bologna, Italy
C. Battilana[a,b], D. Bonacorsi[a,b], L. Borgonovi[a], R. Campanini[a,b], P. Capiluppi[a,b], A. Castro[a,b], F.R. Cavallo[a], M. Cuffiani[a,b], G.M. Dallavalle[a], T. Diotalevi[a,b], F. Fabbri[a], A. Fanfani[a,b], D. Fasanella[a,b], P. Giacomelli[a], L. Giommi[a,b], C. Grandi[a], L. Guiducci[a,b], S. Lo Meo[a,48], L. Lunerti[a,b], S. Marcellini[a], G. Masetti[a], F.L. Navarria[a,b], A. Perrotta[a], F. Primavera[a,b], A.M. Rossi[a,b], T. Rovelli[a,b], G.P. Siroli[a,b]

INFN Sezione di Catania[a], Università di Catania[b], Catania, Italy
S. Costa[a,b,49], A. Di Mattia[a], R. Potenza[a,b], A. Tricomi[a,b,49], C. Tuve[a,b]

INFN Sezione di Firenze[a], Università di Firenze[b], Firenze, Italy
G. Barbagli[a], G. Bardelli[a,b], B. Camaiani[a,b], A. Cassese[a], R. Ceccarelli[a], V. Ciulli[a,b], C. Civinini[a], R. D'Alessandro[a,b], E. Focardi[a,b], T. Kello[a], G. Latino[a,b], P. Lenzi[a,b], M. Lizzo[a], M. Meschini[a], S. Paoletti[a], A. Papanastassiou[a,b], G. Sguazzoni[a], L. Viliani[a]

INFN Laboratori Nazionali di Frascati, Frascati, Italy
L. Benussi, S. Bianco, S. Meola[50], D. Piccolo

INFN Sezione di Genova[a], Università di Genova[b], Genova, Italy
P. Chatagnon[a], F. Ferro[a], E. Robutti[a], S. Tosi[a,b]

INFN Sezione di Milano-Bicocca[a], Università di Milano-Bicocca[b], Milano, Italy
A. Benaglia[a], G. Boldrini[a,b], F. Brivio[a], F. Cetorelli[a], F. De Guio[a,b], M.E. Dinardo[a,b], P. Dini[a], S. Gennai[a], R. Gerosa[a,b], A. Ghezzi[a,b], P. Govoni[a,b],

L. Guzzi[a], M.T. Lucchini[a,b], M. Malberti[a], S. Malvezzi[a], A. Massironi[a], D. Menasce[a], L. Moroni[a], M. Paganoni[a,b], D. Pedrini[a], B.S. Pinolini[a], S. Ragazzi[a,b], T. Tabarelli de Fatis[a,b], D. Zuolo[a]

INFN Sezione di Napoli[a], Università di Napoli 'Federico II'[b], Napoli, Italy; Università della Basilicata[c], Potenza, Italy; Scuola Superiore Meridionale (SSM)[d], Napoli, Italy
S. Buontempo[a], A. Cagnotta[a,b], F. Carnevali[a,b], N. Cavallo[a,c], A. De Iorio[a,b], F. Fabozzi[a,c], A.O.M. Iorio[a,b], L. Lista[a,b,51], P. Paolucci[a,31], B. Rossi[a], C. Sciacca[a,b]

INFN Sezione di Padova[a], Università di Padova[b], Padova, Italy; Università di Trento[c], Trento, Italy
R. Ardino[a], P. Azzi[a], N. Bacchetta[a,52], M. Bellato[a], M. Benettoni[a], D. Bisello[a,b], P. Bortignon[a], A. Bragagnolo[a,b], R. Carlin[a,b], T. Dorigo[a], F. Gasparini[a,b], U. Gasparini[a,b], G. Grosso[a], L. Layer[a,53], E. Lusiani[a], M. Margoni[a,b], M. Migliorini[a,b], J. Pazzini[a,b], P. Ronchese[a,b], R. Rossin[a,b], F. Simonetto[a,b], G. Strong[a], M. Tosi[a,b], A. Triossi[a,b], S. Ventura[a], H. Yarar[a,b], M. Zanetti[a,b], P. Zotto[a,b], A. Zucchetta[a,b], G. Zumerle[a,b]

INFN Sezione di Pavia[a], Università di Pavia[b], Pavia, Italy
S. Abu Zeid[a,54], C. Aimè[a,b], A. Braghieri[a], S. Calzaferri[a,b], D. Fiorina[a,b], P. Montagna[a,b], V. Re[a], C. Riccardi[a,b], P. Salvini[a], I. Vai[a,b], P. Vitulo[a,b]

INFN Sezione di Perugia[a], Università di Perugia[b], Perugia, Italy
S. Ajmal[a,b], P. Asenov[a,55], G.M. Bilei[a], D. Ciangottini[a,b], L. Fanò[a,b], M. Magherini[a,b], G. Mantovani[a,b], V. Mariani[a,b], M. Menichelli[a], F. Moscatelli[a,55], A. Piccinelli[a,b], M. Presilla[a,b], A. Rossi[a,b], A. Santocchia[a,b], D. Spiga[a], T. Tedeschi[a,b]

INFN Sezione di Pisa[a], Università di Pisa[b], Scuola Normale Superiore di Pisa[c], Pisa, Italy; Università di Siena[d], Siena, Italy
P. Azzurri[a], G. Bagliesi[a], R. Bhattacharya[a], L. Bianchini[a,b], T. Boccali[a], E. Bossini[a], D. Bruschini[a,c], R. Castaldi[a], M.A. Ciocci[a,b], M. Cipriani[a,b], V. D'Amante[a,d], R. Dell'Orso[a], S. Donato[a], A. Giassi[a], F. Ligabue[a,c], D. Matos Figueiredo[a], A. Messineo[a,b], M. Musich[a,b], F. Palla[a], A. Rizzi[a,b], G. Rolandi[a,c], S. Roy Chowdhury[a], T. Sarkar[a], A. Scribano[a], P. Spagnolo[a], R. Tenchini[a], G. Tonelli[a,b], N. Turini[a,d], A. Venturi[a], P.G. Verdini[a]

INFN Sezione di Roma[a], Sapienza Università di Roma[b], Roma, Italy
P. Barria[a], M. Campana[a,b], F. Cavallari[a], L. Cunqueiro Mendez[a,b], D. Del Re[a,b], E. Di Marco[a], M. Diemoz[a], F. Errico[a,b], E. Longo[a,b], P. Meridiani[a], J. Mijuskovic[a,b], G. Organtini[a,b], F. Pandolfi[a], R. Paramatti[a,b], C. Quaranta[a,b], S. Rahatlou[a,b], C. Rovelli[a], F. Santanastasio[a,b], L. Soffi[a]

INFN Sezione di Torino[a], Università di Torino[b], Torino, Italy; Università del Piemonte Orientale[c], Novara, Italy
N. Amapane[a,b], R. Arcidiacono[a,c], S. Argiro[a,b], M. Arneodo[a,c], N. Bartosik[a], R. Bellan[a,b], A. Bellora[a,b], C. Biino[a], N. Cartiglia[a], M. Costa[a,b], R. Covarelli[a,b], N. Demaria[a], L. Finco[a], M. Grippo[a,b], B. Kiani[a,b], F. Legger[a], F. Luongo[a,b], C. Mariotti[a], S. Maselli[a], A. Mecca[a,b], E. Migliore[a,b], M. Monteno[a], R. Mulargia[a], M.M. Obertino[a,b], G. Ortona[a], L. Pacher[a,b], N. Pastrone[a], M. Pelliccioni[a], M. Ruspa[a,c], F. Siviero[a,b], V. Sola[a,b], A. Solano[a,b], D. Soldi[a,b], A. Staiano[a], C. Tarricone[a,b], M. Tornago[a,b], D. Trocino[a], G. Umoret[a,b],

E. Vlasov[a,b]

INFN Sezione di Trieste[a], Università di Trieste[b], Trieste, Italy
S. Belforte[a], V. Candelise[a,b], M. Casarsa[a], F. Cossutti[a], K. De Leo[a,b], G. Della Ricca[a,b]

Kyungpook National University, Daegu, Korea
S. Dogra, J. Hong, C. Huh, B. Kim, D.H. Kim, J. Kim, H. Lee, S.W. Lee, C.S. Moon, Y.D. Oh, M.S. Ryu, S. Sekmen, Y.C. Yang

Chonnam National University, Institute for Universe and Elementary Particles, Kwangju, Korea
G. Bak, P. Gwak, H. Kim, D.H. Moon

Hanyang University, Seoul, Korea
E. Asilar, D. Kim, T.J. Kim, J.A. Merlin, J. Park

Korea University, Seoul, Korea
S. Choi, S. Han, B. Hong, K. Lee, K.S. Lee, S. Lee, J. Park, S.K. Park, J. Yoo

Kyung Hee University, Department of Physics, Seoul, Korea
J. Goh

Sejong University, Seoul, Korea
H. S. Kim, Y. Kim, S. Lee

Seoul National University, Seoul, Korea
J. Almond, J.H. Bhyun, J. Choi, W. Jun, J. Kim, J.S. Kim, S. Ko, H. Kwon, H. Lee, J. Lee, J. Lee, B.H. Oh, S.B. Oh, H. Seo, U.K. Yang, I. Yoon

University of Seoul, Seoul, Korea
W. Jang, D.Y. Kang, Y. Kang, S. Kim, B. Ko, J.S.H. Lee, Y. Lee, I.C. Park, Y. Roh, I.J. Watson, S. Yang

Yonsei University, Department of Physics, Seoul, Korea
S. Ha, H.D. Yoo

Sungkyunkwan University, Suwon, Korea
M. Choi, M.R. Kim, H. Lee, Y. Lee, I. Yu

College of Engineering and Technology, American University of the Middle East (AUM), Dasman, Kuwait
T. Beyrouthy, Y. Maghrbi

Riga Technical University, Riga, Latvia
K. Dreimanis, A. Gaile, G. Pikurs, A. Potrebko, M. Seidel, V. Veckalns[56]

University of Latvia (LU), Riga, Latvia
N.R. Strautnieks

Vilnius University, Vilnius, Lithuania
M. Ambrozas, A. Juodagalvis, A. Rinkevicius, G. Tamulaitis

National Centre for Particle Physics, Universiti Malaya, Kuala Lumpur, Malaysia
N. Bin Norjoharuddeen, I. Yusuff[57], Z. Zolkapli

Universidad de Sonora (UNISON), Hermosillo, Mexico
J.F. Benitez, A. Castaneda Hernandez, H.A. Encinas Acosta, L.G. Gallegos Maríñez,

M. León Coello, J.A. Murillo Quijada, A. Sehrawat, L. Valencia Palomo

Centro de Investigacion y de Estudios Avanzados del IPN, Mexico City, Mexico
G. Ayala, H. Castilla-Valdez, E. De La Cruz-Burelo, I. Heredia-De La Cruz[58], R. Lopez-Fernandez, C.A. Mondragon Herrera, A. Sánchez Hernández

Universidad Iberoamericana, Mexico City, Mexico
C. Oropeza Barrera, M. Ramírez García

Benemerita Universidad Autonoma de Puebla, Puebla, Mexico
I. Bautista, I. Pedraza, H.A. Salazar Ibarguen, C. Uribe Estrada

University of Montenegro, Podgorica, Montenegro
I. Bubanja, N. Raicevic

University of Canterbury, Christchurch, New Zealand
P.H. Butler

National Centre for Physics, Quaid-I-Azam University, Islamabad, Pakistan
A. Ahmad, M.I. Asghar, A. Awais, M.I.M. Awan, H.R. Hoorani, W.A. Khan

AGH University of Krakow, Faculty of Computer Science, Electronics and Telecommunications, Krakow, Poland
V. Avati, L. Grzanka, M. Malawski

National Centre for Nuclear Research, Swierk, Poland
H. Bialkowska, M. Bluj, B. Boimska, M. Górski, M. Kazana, M. Szleper, P. Zalewski

Institute of Experimental Physics, Faculty of Physics, University of Warsaw, Warsaw, Poland
K. Bunkowski, K. Doroba, A. Kalinowski, M. Konecki, J. Krolikowski, A. Muhammad

Warsaw University of Technology, Warsaw, Poland
K. Pozniak, W. Zabolotny

Laboratório de Instrumentação e Física Experimental de Partículas, Lisboa, Portugal
M. Araujo, D. Bastos, C. Beirão Da Cruz E Silva, A. Boletti, M. Bozzo, P. Faccioli, M. Gallinaro, J. Hollar, N. Leonardo, T. Niknejad, A. Petrilli, M. Pisano, J. Seixas, J. Varela, J.W. Wulff

Faculty of Physics, University of Belgrade, Belgrade, Serbia
P. Adzic, P. Milenovic

VINCA Institute of Nuclear Sciences, University of Belgrade, Belgrade, Serbia
M. Dordevic, J. Milosevic, V. Rekovic

Centro de Investigaciones Energéticas Medioambientales y Tecnológicas (CIEMAT), Madrid, Spain
M. Aguilar-Benitez, J. Alcaraz Maestre, Cristina F. Bedoya, M. Cepeda, M. Cerrada, N. Colino, B. De La Cruz, A. Delgado Peris, D. Fernández Del Val, J.P. Fernández Ramos, J. Flix, M.C. Fouz, O. Gonzalez Lopez, S. Goy Lopez, J.M. Hernandez, M.I. Josa, J. León Holgado, D. Moran, C. M. Morcillo Perez, Á. Navarro Tobar, C. Perez Dengra, A. Pérez-Calero Yzquierdo, J. Puerta Pelayo, I. Redondo, D.D. Redondo Ferrero, L. Romero, S. Sánchez Navas, L. Urda Gómez, J. Vazquez Escobar, C. Willmott

Universidad Autónoma de Madrid, Madrid, Spain
J.F. de Trocóniz

Universidad de Oviedo, Instituto Universitario de Ciencias y Tecnologías Espaciales de Asturias (ICTEA), Oviedo, Spain
B. Alvarez Gonzalez, J. Cuevas, J. Fernandez Menendez, S. Folgueras, I. Gonzalez Caballero, J.R. González Fernández, E. Palencia Cortezon, C. Ramón Álvarez, V. Rodríguez Bouza, A. Soto Rodríguez, A. Trapote, C. Vico Villalba, P. Vischia

Instituto de Física de Cantabria (IFCA), CSIC-Universidad de Cantabria, Santander, Spain
S. Bhowmik, S. Blanco Fernández, J.A. Brochero Cifuentes, I.J. Cabrillo, A. Calderon, J. Duarte Campderros, M. Fernandez, C. Fernandez Madrazo, G. Gomez, C. Lasaosa García, C. Martinez Rivero, P. Martinez Ruiz del Arbol, F. Matorras, P. Matorras Cuevas, E. Navarrete Ramos, J. Piedra Gomez, L. Scodellaro, I. Vila, J.M. Vizan Garcia

University of Colombo, Colombo, Sri Lanka
M.K. Jayananda, B. Kailasapathy[59], D.U.J. Sonnadara, D.D.C. Wickramarathna

University of Ruhuna, Department of Physics, Matara, Sri Lanka
W.G.D. Dharmaratna[60], K. Liyanage, N. Perera, N. Wickramage

CERN, European Organization for Nuclear Research, Geneva, Switzerland
D. Abbaneo, C. Amendola, E. Auffray, G. Auzinger, J. Baechler, D. Barney, A. Bermúdez Martínez, M. Bianco, B. Bilin, A.A. Bin Anuar, A. Bocci, E. Brondolin, C. Caillol, T. Camporesi, G. Cerminara, N. Chernyavskaya, D. d'Enterria, A. Dabrowski, A. David, A. De Roeck, M.M. Defranchis, M. Deile, M. Dobson, F. Fallavollita[61], L. Forthomme, G. Franzoni, W. Funk, S. Giani, D. Gigi, K. Gill, F. Glege, L. Gouskos, M. Haranko, J. Hegeman, B. Huber, V. Innocente, T. James, P. Janot, J. Kieseler, S. Laurila, P. Lecoq, E. Leutgeb, C. Lourenço, B. Maier, L. Malgeri, M. Mannelli, A.C. Marini, M. Matthewman, F. Meijers, S. Mersi, E. Meschi, V. Milosevic, F. Moortgat, M. Mulders, S. Orfanelli, F. Pantaleo, M. Peruzzi, G. Petrucciani, A. Pfeiffer, M. Pierini, D. Piparo, H. Qu, D. Rabady, G. Reales Gutiérrez, M. Rovere, H. Sakulin, S. Scarfi, C. Schwick, M. Selvaggi, A. Sharma, K. Shchelina, P. Silva, P. Sphicas[62], A.G. Stahl Leiton, A. Steen, S. Summers, D. Treille, P. Tropea, A. Tsirou, D. Walter, J. Wanczyk[63], K.A. Wozniak[64], P. Zehetner, P. Zejdl, W.D. Zeuner

Paul Scherrer Institut, Villigen, Switzerland
T. Bevilacqua[65], L. Caminada[65], A. Ebrahimi, W. Erdmann, R. Horisberger, Q. Ingram, H.C. Kaestli, D. Kotlinski, C. Lange, M. Missiroli[65], L. Noehte[65], T. Rohe

ETH Zurich - Institute for Particle Physics and Astrophysics (IPA), Zurich, Switzerland
T.K. Aarrestad, K. Androsov[63], M. Backhaus, A. Calandri, C. Cazzaniga, K. Datta, A. De Cosa, G. Dissertori, M. Dittmar, M. Donegà, F. Eble, M. Galli, K. Gedia, F. Glessgen, C. Grab, D. Hits, W. Lustermann, A.-M. Lyon, R.A. Manzoni, M. Marchegiani, L. Marchese, C. Martin Perez, A. Mascellani[63], F. Nessi-Tedaldi, F. Pauss, V. Perovic, S. Pigazzini, M.G. Ratti, M. Reichmann, C. Reissel, T. Reitenspiess, B. Ristic, F. Riti, D. Ruini, D.A. Sanz Becerra, R. Seidita, J. Steggemann[63], D. Valsecchi, R. Wallny

Universität Zürich, Zurich, Switzerland

C. Amsler[66], P. Bärtschi, C. Botta, D. Brzhechko, M.F. Canelli, K. Cormier, R. Del Burgo, J.K. Heikkilä, M. Huwiler, W. Jin, A. Jofrehei, B. Kilminster, S. Leontsinis, S.P. Liechti, A. Macchiolo, P. Meiring, V.M. Mikuni, U. Molinatti, I. Neutelings, A. Reimers, P. Robmann, S. Sanchez Cruz, K. Schweiger, M. Senger, Y. Takahashi, R. Tramontano

National Central University, Chung-Li, Taiwan
C. Adloff[67], C.M. Kuo, W. Lin, P.K. Rout, P.C. Tiwari[41], S.S. Yu

National Taiwan University (NTU), Taipei, Taiwan
L. Ceard, Y. Chao, K.F. Chen, P.s. Chen, Z.g. Chen, W.-S. Hou, T.h. Hsu, Y.w. Kao, R. Khurana, G. Kole, Y.y. Li, R.-S. Lu, E. Paganis, A. Psallidas, X.f. Su, J. Thomas-Wilsker, H.y. Wu, E. Yazgan

High Energy Physics Research Unit, Department of Physics, Faculty of Science, Chulalongkorn University, Bangkok, Thailand
C. Asawatangtrakuldee, N. Srimanobhas, V. Wachirapusitanand

Çukurova University, Physics Department, Science and Art Faculty, Adana, Turkey
D. Agyel, F. Boran, Z.S. Demiroglu, F. Dolek, I. Dumanoglu[68], E. Eskut, Y. Guler[69], E. Gurpinar Guler[69], C. Isik, O. Kara, A. Kayis Topaksu, U. Kiminsu, G. Onengut, K. Ozdemir[70], A. Polatoz, B. Tali[71], U.G. Tok, S. Turkcapar, E. Uslan, I.S. Zorbakir

Middle East Technical University, Physics Department, Ankara, Turkey
M. Yalvac[72]

Bogazici University, Istanbul, Turkey
B. Akgun, I.O. Atakisi, E. Gülmez, M. Kaya[73], O. Kaya[74], S. Tekten[75]

Istanbul Technical University, Istanbul, Turkey
A. Cakir, K. Cankocak[68,76], Y. Komurcu, S. Sen[77]

Istanbul University, Istanbul, Turkey
O. Aydilek, S. Cerci[71], V. Epshteyn, B. Hacisahinoglu, I. Hos[78], B. Isildak[79], B. Kaynak, S. Ozkorucuklu, O. Potok, H. Sert, C. Simsek, D. Sunar Cerci[71], C. Zorbilmez

Institute for Scintillation Materials of National Academy of Science of Ukraine, Kharkiv, Ukraine
A. Boyaryntsev, B. Grynyov

National Science Centre, Kharkiv Institute of Physics and Technology, Kharkiv, Ukraine
L. Levchuk

University of Bristol, Bristol, United Kingdom
D. Anthony, J.J. Brooke, A. Bundock, F. Bury, E. Clement, D. Cussans, H. Flacher, M. Glowacki, J. Goldstein, H.F. Heath, L. Kreczko, B. Krikler, S. Paramesvaran, S. Seif El Nasr-Storey, V.J. Smith, N. Stylianou[80], K. Walkingshaw Pass, R. White

Rutherford Appleton Laboratory, Didcot, United Kingdom
A.H. Ball, K.W. Bell, A. Belyaev[81], C. Brew, R.M. Brown, D.J.A. Cockerill, C. Cooke, K.V. Ellis, K. Harder, S. Harper, M.-L. Holmberg[82], J. Linacre, K. Manolopoulos, D.M. Newbold, E. Olaiya, D. Petyt, T. Reis, G. Salvi, T. Schuh,

C.H. Shepherd-Themistocleous, I.R. Tomalin, T. Williams

Imperial College, London, United Kingdom
R. Bainbridge, P. Bloch, C.E. Brown, O. Buchmuller, V. Cacchio, C.A. Carrillo Montoya, G.S. Chahal[83], D. Colling, J.S. Dancu, P. Dauncey, G. Davies, J. Davies, M. Della Negra, S. Fayer, G. Fedi, G. Hall, M.H. Hassanshahi, A. Howard, G. Iles, M. Knight, J. Langford, L. Lyons, A.-M. Magnan, S. Malik, A. Martelli, M. Mieskolainen, J. Nash[84], M. Pesaresi, B.C. Radburn-Smith, A. Richards, A. Rose, C. Seez, R. Shukla, A. Tapper, K. Uchida, G.P. Uttley, L.H. Vage, T. Virdee[31], M. Vojinovic, N. Wardle, D. Winterbottom

Brunel University, Uxbridge, United Kingdom
K. Coldham, J.E. Cole, A. Khan, P. Kyberd, I.D. Reid

Baylor University, Waco, Texas, USA
S. Abdullin, A. Brinkerhoff, B. Caraway, J. Dittmann, K. Hatakeyama, J. Hiltbrand, A.R. Kanuganti, B. McMaster, M. Saunders, S. Sawant, C. Sutantawibul, M. Toms[85], J. Wilson

Catholic University of America, Washington, DC, USA
R. Bartek, A. Dominguez, C. Huerta Escamilla, A.E. Simsek, R. Uniyal, A.M. Vargas Hernandez

The University of Alabama, Tuscaloosa, Alabama, USA
R. Chudasama, S.I. Cooper, S.V. Gleyzer, C.U. Perez, P. Rumerio[86], E. Usai, C. West, R. Yi

Boston University, Boston, Massachusetts, USA
A. Akpinar, A. Albert, D. Arcaro, C. Cosby, Z. Demiragli, C. Erice, E. Fontanesi, D. Gastler, S. Jeon, J. Rohlf, K. Salyer, D. Sperka, D. Spitzbart, I. Suarez, A. Tsatsos, S. Yuan

Brown University, Providence, Rhode Island, USA
G. Benelli, X. Coubez[26], D. Cutts, M. Hadley, U. Heintz, J.M. Hogan[87], T. Kwon, G. Landsberg, K.T. Lau, D. Li, J. Luo, S. Mondal, M. Narain[†], N. Pervan, S. Sagir[88], F. Simpson, M. Stamenkovic, W.Y. Wong, X. Yan, W. Zhang

University of California, Davis, Davis, California, USA
S. Abbott, J. Bonilla, C. Brainerd, R. Breedon, M. Calderon De La Barca Sanchez, M. Chertok, M. Citron, J. Conway, P.T. Cox, R. Erbacher, F. Jensen, O. Kukral, G. Mocellin, M. Mulhearn, D. Pellett, W. Wei, Y. Yao, F. Zhang

University of California, Los Angeles, California, USA
M. Bachtis, R. Cousins, A. Datta, J. Hauser, M. Ignatenko, M.A. Iqbal, T. Lam, E. Manca, W.A. Nash, D. Saltzberg, B. Stone, V. Valuev

University of California, Riverside, Riverside, California, USA
R. Clare, M. Gordon, G. Hanson, W. Si, S. Wimpenny[†]

University of California, San Diego, La Jolla, California, USA
J.G. Branson, S. Cittolin, S. Cooperstein, D. Diaz, J. Duarte, L. Giannini, J. Guiang, R. Kansal, V. Krutelyov, R. Lee, J. Letts, M. Masciovecchio, F. Mokhtar, M. Pieri, M. Quinnan, B.V. Sathia Narayanan, V. Sharma, M. Tadel, E. Vourliotis, F. Würthwein, Y. Xiang, A. Yagil

University of California, Santa Barbara - Department of Physics, Santa Barbara, California, USA
A. Barzdukas, L. Brennan, C. Campagnari, G. Collura, A. Dorsett, J. Incandela, M. Kilpatrick, J. Kim, A.J. Li, P. Masterson, H. Mei, M. Oshiro, J. Richman, U. Sarica, R. Schmitz, F. Setti, J. Sheplock, D. Stuart, S. Wang

California Institute of Technology, Pasadena, California, USA
A. Bornheim, O. Cerri, A. Latorre, J.M. Lawhorn, J. Mao, H.B. Newman, T. Q. Nguyen, M. Spiropulu, J.R. Vlimant, C. Wang, S. Xie, R.Y. Zhu

Carnegie Mellon University, Pittsburgh, Pennsylvania, USA
J. Alison, S. An, M.B. Andrews, P. Bryant, V. Dutta, T. Ferguson, A. Harilal, C. Liu, T. Mudholkar, S. Murthy, M. Paulini, A. Roberts, A. Sanchez, W. Terrill

University of Colorado Boulder, Boulder, Colorado, USA
J.P. Cumalat, W.T. Ford, A. Hassani, G. Karathanasis, E. MacDonald, N. Manganelli, F. Marini, A. Perloff, C. Savard, N. Schonbeck, K. Stenson, K.A. Ulmer, S.R. Wagner, N. Zipper

Cornell University, Ithaca, New York, USA
J. Alexander, S. Bright-Thonney, X. Chen, D.J. Cranshaw, J. Fan, X. Fan, D. Gadkari, S. Hogan, J. Monroy, J.R. Patterson, J. Reichert, M. Reid, A. Ryd, J. Thom, P. Wittich, R. Zou

Fermi National Accelerator Laboratory, Batavia, Illinois, USA
M. Albrow, M. Alyari, O. Amram, G. Apollinari, A. Apresyan, L.A.T. Bauerdick, D. Berry, J. Berryhill, P.C. Bhat, K. Burkett, J.N. Butler, A. Canepa, G.B. Cerati, H.W.K. Cheung, F. Chlebana, G. Cummings, J. Dickinson, I. Dutta, V.D. Elvira, Y. Feng, J. Freeman, A. Gandrakota, Z. Gecse, L. Gray, D. Green, A. Grummer, S. Grünendahl, D. Guerrero, O. Gutsche, R.M. Harris, R. Heller, T.C. Herwig, J. Hirschauer, L. Horyn, B. Jayatilaka, S. Jindariani, M. Johnson, U. Joshi, T. Klijnsma, B. Klima, K.H.M. Kwok, S. Lammel, D. Lincoln, R. Lipton, T. Liu, C. Madrid, K. Maeshima, C. Mantilla, D. Mason, P. McBride, P. Merkel, S. Mrenna, S. Nahn, J. Ngadiuba, D. Noonan, V. Papadimitriou, N. Pastika, K. Pedro, C. Pena[89], F. Ravera, A. Reinsvold Hall[90], L. Ristori, E. Sexton-Kennedy, N. Smith, A. Soha, L. Spiegel, S. Stoynev, J. Strait, L. Taylor, S. Tkaczyk, N.V. Tran, L. Uplegger, E.W. Vaandering, I. Zoi

University of Florida, Gainesville, Florida, USA
C. Aruta, P. Avery, D. Bourilkov, L. Cadamuro, P. Chang, V. Cherepanov, R.D. Field, E. Koenig, M. Kolosova, J. Konigsberg, A. Korytov, K.H. Lo, K. Matchev, N. Menendez, G. Mitselmakher, A. Muthirakalayil Madhu, N. Rawal, D. Rosenzweig, S. Rosenzweig, K. Shi, J. Wang

Florida State University, Tallahassee, Florida, USA
T. Adams, A. Al Kadhim, A. Askew, N. Bower, R. Habibullah, V. Hagopian, R. Hashmi, R.S. Kim, S. Kim, T. Kolberg, G. Martinez, H. Prosper, P.R. Prova, O. Viazlo, M. Wulansatiti, R. Yohay, J. Zhang

Florida Institute of Technology, Melbourne, Florida, USA
B. Alsufyani, M.M. Baarmand, S. Butalla, T. Elkafrawy[54], M. Hohlmann, R. Kumar Verma, M. Rahmani

University of Illinois Chicago, Chicago, USA, Chicago, USA

M.R. Adams, C. Bennett, R. Cavanaugh, S. Dittmer, R. Escobar Franco, O. Evdokimov, C.E. Gerber, D.J. Hofman, J.h. Lee, D. S. Lemos, A.H. Merrit, C. Mills, S. Nanda, G. Oh, B. Ozek, D. Pilipovic, T. Roy, S. Rudrabhatla, M.B. Tonjes, N. Varelas, X. Wang, Z. Ye, J. Yoo

The University of Iowa, Iowa City, Iowa, USA
M. Alhusseini, D. Blend, K. Dilsiz[91], L. Emediato, G. Karaman, O.K. Köseyan, J.-P. Merlo, A. Mestvirishvili[92], J. Nachtman, O. Neogi, H. Ogul[93], Y. Onel, A. Penzo, C. Snyder, E. Tiras[94]

Johns Hopkins University, Baltimore, Maryland, USA
B. Blumenfeld, L. Corcodilos, J. Davis, A.V. Gritsan, L. Kang, S. Kyriacou, P. Maksimovic, M. Roguljic, J. Roskes, S. Sekhar, M. Swartz, T.Á. Vámi

The University of Kansas, Lawrence, Kansas, USA
A. Abreu, L.F. Alcerro Alcerro, J. Anguiano, P. Baringer, A. Bean, Z. Flowers, D. Grove, J. King, G. Krintiras, M. Lazarovits, C. Le Mahieu, C. Lindsey, J. Marquez, N. Minafra, M. Murray, M. Nickel, M. Pitt, S. Popescu[95], C. Rogan, C. Royon, R. Salvatico, S. Sanders, C. Smith, Q. Wang, G. Wilson

Kansas State University, Manhattan, Kansas, USA
B. Allmond, A. Ivanov, K. Kaadze, A. Kalogeropoulos, D. Kim, Y. Maravin, K. Nam, J. Natoli, D. Roy, G. Sorrentino

Lawrence Livermore National Laboratory, Livermore, California, USA
F. Rebassoo, D. Wright

University of Maryland, College Park, Maryland, USA
E. Adams, A. Baden, O. Baron, A. Belloni, A. Bethani, Y.M. Chen, S.C. Eno, N.J. Hadley, S. Jabeen, R.G. Kellogg, T. Koeth, Y. Lai, S. Lascio, A.C. Mignerey, S. Nabili, C. Palmer, C. Papageorgakis, M.M. Paranjpe, L. Wang, K. Wong

Massachusetts Institute of Technology, Cambridge, Massachusetts, USA
J. Bendavid, W. Busza, I.A. Cali, Y. Chen, M. D'Alfonso, J. Eysermans, C. Freer, G. Gomez-Ceballos, M. Goncharov, P. Harris, D. Hoang, D. Kovalskyi, J. Krupa, L. Lavezzo, Y.-J. Lee, K. Long, C. Mironov, C. Paus, D. Rankin, C. Roland, G. Roland, S. Rothman, Z. Shi, G.S.F. Stephans, J. Wang, Z. Wang, B. Wyslouch, T. J. Yang

University of Minnesota, Minneapolis, Minnesota, USA
B. Crossman, B.M. Joshi, C. Kapsiak, M. Krohn, D. Mahon, J. Mans, B. Marzocchi, S. Pandey, M. Revering, R. Rusack, R. Saradhy, N. Schroeder, N. Strobbe, M.A. Wadud

University of Mississippi, Oxford, Mississippi, USA
L.M. Cremaldi

University of Nebraska-Lincoln, Lincoln, Nebraska, USA
K. Bloom, M. Bryson, D.R. Claes, C. Fangmeier, F. Golf, G. Haza, J. Hossain, C. Joo, I. Kravchenko, I. Reed, J.E. Siado, W. Tabb, A. Vagnerini, A. Wightman, F. Yan, D. Yu, A.G. Zecchinelli

State University of New York at Buffalo, Buffalo, New York, USA
G. Agarwal, H. Bandyopadhyay, L. Hay, I. Iashvili, A. Kharchilava, C. McLean, M. Morris, D. Nguyen, S. Rappoccio, H. Rejeb Sfar, A. Williams

Northeastern University, Boston, Massachusetts, USA
G. Alverson, E. Barberis, Y. Haddad, Y. Han, A. Krishna, J. Li, M. Lu, G. Madigan, D.M. Morse, V. Nguyen, T. Orimoto, A. Parker, L. Skinnari, A. Tishelman-Charny, B. Wang, D. Wood

Northwestern University, Evanston, Illinois, USA
S. Bhattacharya, J. Bueghly, Z. Chen, K.A. Hahn, Y. Liu, Y. Miao, D.G. Monk, M.H. Schmitt, A. Taliercio, M. Velasco

University of Notre Dame, Notre Dame, Indiana, USA
R. Band, R. Bucci, S. Castells, M. Cremonesi, A. Das, R. Goldouzian, M. Hildreth, K.W. Ho, K. Hurtado Anampa, C. Jessop, K. Lannon, J. Lawrence, N. Loukas, L. Lutton, J. Mariano, N. Marinelli, I. Mcalister, T. McCauley, C. Mcgrady, K. Mohrman, C. Moore, Y. Musienko[16], H. Nelson, M. Osherson, R. Ruchti, A. Townsend, M. Wayne, H. Yockey, M. Zarucki, L. Zygala

The Ohio State University, Columbus, Ohio, USA
A. Basnet, B. Bylsma, M. Carrigan, L.S. Durkin, C. Hill, M. Joyce, A. Lesauvage, M. Nunez Ornelas, K. Wei, B.L. Winer, B. R. Yates

Princeton University, Princeton, New Jersey, USA
F.M. Addesa, H. Bouchamaoui, P. Das, G. Dezoort, P. Elmer, A. Frankenthal, B. Greenberg, N. Haubrich, S. Higginbotham, G. Kopp, S. Kwan, D. Lange, A. Loeliger, D. Marlow, I. Ojalvo, J. Olsen, D. Stickland, C. Tully

University of Puerto Rico, Mayaguez, Puerto Rico, USA
S. Malik

Purdue University, West Lafayette, Indiana, USA
A.S. Bakshi, V.E. Barnes, S. Chandra, R. Chawla, S. Das, A. Gu, L. Gutay, M. Jones, A.W. Jung, D. Kondratyev, A.M. Koshy, M. Liu, G. Negro, N. Neumeister, G. Paspalaki, S. Piperov, V. Scheurer, J.F. Schulte, M. Stojanovic, J. Thieman, A. K. Virdi, F. Wang, W. Xie

Purdue University Northwest, Hammond, Indiana, USA
J. Dolen, N. Parashar, A. Pathak

Rice University, Houston, Texas, USA
D. Acosta, A. Baty, T. Carnahan, S. Dildick, K.M. Ecklund, P.J. Fernández Manteca, S. Freed, P. Gardner, F.J.M. Geurts, A. Kumar, W. Li, O. Miguel Colin, B.P. Padley, R. Redjimi, J. Rotter, E. Yigitbasi, Y. Zhang

University of Rochester, Rochester, New York, USA
A. Bodek, P. de Barbaro, R. Demina, J.L. Dulemba, C. Fallon, A. Garcia-Bellido, O. Hindrichs, A. Khukhunaishvili, P. Parygin[85], E. Popova[85], R. Taus, G.P. Van Onsem

The Rockefeller University, New York, New York, USA
K. Goulianos

Rutgers, The State University of New Jersey, Piscataway, New Jersey, USA
B. Chiarito, J.P. Chou, Y. Gershtein, E. Halkiadakis, A. Hart, M. Heindl, D. Jaroslawski, O. Karacheban[29], I. Laflotte, A. Lath, R. Montalvo, K. Nash, H. Routray, S. Salur, S. Schnetzer, S. Somalwar, R. Stone, S.A. Thayil, S. Thomas, J. Vora, H. Wang

University of Tennessee, Knoxville, Tennessee, USA
H. Acharya, D. Ally, A.G. Delannoy, S. Fiorendi, T. Holmes, N. Karunarathna, L. Lee, E. Nibigira, S. Spanier

Texas A&M University, College Station, Texas, USA
D. Aebi, M. Ahmad, O. Bouhali[96], M. Dalchenko, R. Eusebi, J. Gilmore, T. Huang, T. Kamon[97], H. Kim, S. Luo, S. Malhotra, R. Mueller, D. Overton, D. Rathjens, A. Safonov

Texas Tech University, Lubbock, Texas, USA
N. Akchurin, J. Damgov, V. Hegde, A. Hussain, Y. Kazhykarim, K. Lamichhane, S.W. Lee, A. Mankel, T. Mengke, S. Muthumuni, T. Peltola, I. Volobouev, A. Whitbeck

Vanderbilt University, Nashville, Tennessee, USA
E. Appelt, S. Greene, A. Gurrola, W. Johns, R. Kunnawalkam Elayavalli, A. Melo, F. Romeo, P. Sheldon, S. Tuo, J. Velkovska, J. Viinikainen

University of Virginia, Charlottesville, Virginia, USA
B. Cardwell, B. Cox, J. Hakala, R. Hirosky, A. Ledovskoy, A. Li, C. Neu, C.E. Perez Lara

Wayne State University, Detroit, Michigan, USA
P.E. Karchin

University of Wisconsin - Madison, Madison, Wisconsin, USA
A. Aravind, S. Banerjee, K. Black, T. Bose, S. Dasu, I. De Bruyn, P. Everaerts, C. Galloni, H. He, M. Herndon, A. Herve, C.K. Koraka, A. Lanaro, R. Loveless, J. Madhusudanan Sreekala, A. Mallampalli, A. Mohammadi, S. Mondal, G. Parida, D. Pinna, A. Savin, V. Shang, V. Sharma, W.H. Smith, D. Teague, H.F. Tsoi, W. Vetens, A. Warden

Authors affiliated with an institute or an international laboratory covered by a cooperation agreement with CERN
S. Afanasiev, V. Andreev, Yu. Andreev, T. Aushev, M. Azarkin, A. Babaev, A. Belyaev, V. Blinov[98], E. Boos, V. Borshch, D. Budkouski, V. Bunichev, M. Chadeeva[98], V. Chekhovsky, R. Chistov[98], A. Dermenev, T. Dimova[98], D. Druzhkin[99], M. Dubinin[89], L. Dudko, A. Ershov, G. Gavrilov, V. Gavrilov, S. Gninenko, V. Golovtcov, N. Golubev, I. Golutvin, I. Gorbunov, A. Gribushin, Y. Ivanov, V. Kachanov, L. Kardapoltsev[98], V. Karjavine, A. Karneyeu, V. Kim[98], M. Kirakosyan, D. Kirpichnikov, M. Kirsanov, V. Klyukhin, O. Kodolova[100], D. Konstantinov, V. Korenkov, A. Kozyrev[98], N. Krasnikov, A. Lanev, P. Levchenko[101], N. Lychkovskaya, V. Makarenko, A. Malakhov, V. Matveev[98], V. Murzin, A. Nikitenko[102,100], S. Obraztsov, V. Oreshkin, V. Palichik, V. Perelygin, M. Perfilov, S. Petrushanko, S. Polikarpov[98], V. Popov, O. Radchenko[98], M. Savina, V. Savrin, V. Shalaev, S. Shmatov, S. Shulha, Y. Skovpen[98], S. Slabospitskii, V. Smirnov, D. Sosnov, V. Sulimov, E. Tcherniaev, A. Terkulov, O. Teryaev, I. Tlisova, A. Toropin, L. Uvarov, A. Uzunian, A. Vorobyev†, N. Voytishin, B.S. Yuldashev[103], A. Zarubin, I. Zhizhin, A. Zhokin

†: Deceased
[1]Also at Yerevan State University, Yerevan, Armenia
[2]Also at TU Wien, Vienna, Austria

[3]Also at Institute of Basic and Applied Sciences, Faculty of Engineering, Arab Academy for Science, Technology and Maritime Transport, Alexandria, Egypt
[4]Also at Ghent University, Ghent, Belgium
[5]Also at Universidade Estadual de Campinas, Campinas, Brazil
[6]Also at Federal University of Rio Grande do Sul, Porto Alegre, Brazil
[7]Also at UFMS, Nova Andradina, Brazil
[8]Also at Nanjing Normal University, Nanjing, China
[9]Now at Henan Normal University, Xinxiang, China
[10]Now at The University of Iowa, Iowa City, Iowa, USA
[11]Also at University of Chinese Academy of Sciences, Beijing, China
[12]Also at China Center of Advanced Science and Technology, Beijing, China
[13]Also at University of Chinese Academy of Sciences, Beijing, China
[14]Also at China Spallation Neutron Source, Guangdong, China
[15]Also at Université Libre de Bruxelles, Bruxelles, Belgium
[16]Also at an institute or an international laboratory covered by a cooperation agreement with CERN
[17]Now at British University in Egypt, Cairo, Egypt
[18]Now at Cairo University, Cairo, Egypt
[19]Also at Birla Institute of Technology, Mesra, Mesra, India
[20]Also at Purdue University, West Lafayette, Indiana, USA
[21]Also at Université de Haute Alsace, Mulhouse, France
[22]Also at Department of Physics, Tsinghua University, Beijing, China
[23]Also at The University of the State of Amazonas, Manaus, Brazil
[24]Also at Erzincan Binali Yildirim University, Erzincan, Turkey
[25]Also at University of Hamburg, Hamburg, Germany
[26]Also at RWTH Aachen University, III. Physikalisches Institut A, Aachen, Germany
[27]Also at Isfahan University of Technology, Isfahan, Iran
[28]Also at Bergische University Wuppertal (BUW), Wuppertal, Germany
[29]Also at Brandenburg University of Technology, Cottbus, Germany
[30]Also at Forschungszentrum Jülich, Juelich, Germany
[31]Also at CERN, European Organization for Nuclear Research, Geneva, Switzerland
[32]Also at Institute of Physics, University of Debrecen, Debrecen, Hungary
[33]Also at Institute of Nuclear Research ATOMKI, Debrecen, Hungary
[34]Now at Universitatea Babes-Bolyai - Facultatea de Fizica, Cluj-Napoca, Romania
[35]Also at Physics Department, Faculty of Science, Assiut University, Assiut, Egypt
[36]Also at HUN-REN Wigner Research Centre for Physics, Budapest, Hungary
[37]Also at Faculty of Informatics, University of Debrecen, Debrecen, Hungary
[38]Also at Punjab Agricultural University, Ludhiana, India
[39]Also at University of Hyderabad, Hyderabad, India
[40]Also at University of Visva-Bharati, Santiniketan, India
[41]Also at Indian Institute of Science (IISc), Bangalore, India
[42]Also at IIT Bhubaneswar, Bhubaneswar, India
[43]Also at Institute of Physics, Bhubaneswar, India
[44]Also at Department of Physics, Isfahan University of Technology, Isfahan, Iran
[45]Also at Sharif University of Technology, Tehran, Iran
[46]Also at Department of Physics, University of Science and Technology of Mazandaran, Behshahr, Iran
[47]Also at Helwan University, Cairo, Egypt
[48]Also at Italian National Agency for New Technologies, Energy and Sustainable Economic

Development, Bologna, Italy
[49]Also at Centro Siciliano di Fisica Nucleare e di Struttura Della Materia, Catania, Italy
[50]Also at Università degli Studi Guglielmo Marconi, Roma, Italy
[51]Also at Scuola Superiore Meridionale, Università di Napoli 'Federico II', Napoli, Italy
[52]Also at Fermi National Accelerator Laboratory, Batavia, Illinois, USA
[53]Also at Università di Napoli 'Federico II', Napoli, Italy
[54]Also at Ain Shams University, Cairo, Egypt
[55]Also at Consiglio Nazionale delle Ricerche - Istituto Officina dei Materiali, Perugia, Italy
[56]Also at Riga Technical University, Riga, Latvia
[57]Also at Department of Applied Physics, Faculty of Science and Technology, Universiti Kebangsaan Malaysia, Bangi, Malaysia
[58]Also at Consejo Nacional de Ciencia y Tecnología, Mexico City, Mexico
[59]Also at Trincomalee Campus, Eastern University, Sri Lanka, Nilaveli, Sri Lanka
[60]Also at Saegis Campus, Nugegoda, Sri Lanka
[61]Also at INFN Sezione di Pavia, Università di Pavia, Pavia, Italy
[62]Also at National and Kapodistrian University of Athens, Athens, Greece
[63]Also at Ecole Polytechnique Fédérale Lausanne, Lausanne, Switzerland
[64]Also at University of Vienna Faculty of Computer Science, Vienna, Austria
[65]Also at Universität Zürich, Zurich, Switzerland
[66]Also at Stefan Meyer Institute for Subatomic Physics, Vienna, Austria
[67]Also at Laboratoire d'Annecy-le-Vieux de Physique des Particules, IN2P3-CNRS, Annecy-le-Vieux, France
[68]Also at Near East University, Research Center of Experimental Health Science, Mersin, Turkey
[69]Also at Konya Technical University, Konya, Turkey
[70]Also at Izmir Bakircay University, Izmir, Turkey
[71]Also at Adiyaman University, Adiyaman, Turkey
[72]Also at Bozok Universitetesi Rektörlügü, Yozgat, Turkey
[73]Also at Marmara University, Istanbul, Turkey
[74]Also at Milli Savunma University, Istanbul, Turkey
[75]Also at Kafkas University, Kars, Turkey
[76]Now at stanbul Okan University, Istanbul, Turkey
[77]Also at Hacettepe University, Ankara, Turkey
[78]Also at Istanbul University - Cerrahpasa, Faculty of Engineering, Istanbul, Turkey
[79]Also at Yildiz Technical University, Istanbul, Turkey
[80]Also at Vrije Universiteit Brussel, Brussel, Belgium
[81]Also at School of Physics and Astronomy, University of Southampton, Southampton, United Kingdom
[82]Also at University of Bristol, Bristol, United Kingdom
[83]Also at IPPP Durham University, Durham, United Kingdom
[84]Also at Monash University, Faculty of Science, Clayton, Australia
[85]Now at an institute or an international laboratory covered by a cooperation agreement with CERN
[86]Also at Università di Torino, Torino, Italy
[87]Also at Bethel University, St. Paul, Minnesota, USA
[88]Also at Karamanoğlu Mehmetbey University, Karaman, Turkey
[89]Also at California Institute of Technology, Pasadena, California, USA
[90]Also at United States Naval Academy, Annapolis, Maryland, USA
[91]Also at Bingol University, Bingol, Turkey

[92]Also at Georgian Technical University, Tbilisi, Georgia
[93]Also at Sinop University, Sinop, Turkey
[94]Also at Erciyes University, Kayseri, Turkey
[95]Also at Horia Hulubei National Institute of Physics and Nuclear Engineering (IFIN-HH), Bucharest, Romania
[96]Also at Texas A&M University at Qatar, Doha, Qatar
[97]Also at Kyungpook National University, Daegu, Korea
[98]Also at another institute or international laboratory covered by a cooperation agreement with CERN
[99]Also at Universiteit Antwerpen, Antwerpen, Belgium
[100]Also at Yerevan Physics Institute, Yerevan, Armenia
[101]Also at Northeastern University, Boston, Massachusetts, USA
[102]Also at Imperial College, London, United Kingdom
[103]Also at Institute of Nuclear Physics of the Uzbekistan Academy of Sciences, Tashkent, Uzbekistan